# Integrated Multi-Mission Ocean Altimeter Data for Climate Research TOPEX/Poseidon, Jason-1, 2, & 3

# User's Handbook

# Version 4.0

# Table of Contents



# Table of Figures

| | |
|---|---|
| Brian Beckley | SGT, Inc. |
| Richard Ray | NASA/GSFC |
| Simon Holmes | SGT, Inc. |
| Nikita Zelensky | SGT, Inc. |
| Frank Lemoine | NASA/GSFC |
| Xu Yang | SGT, Inc. |
| Shannon Brown | JPL/Caltech/NASA |
| Shailen Desai | JPL/Caltech/NASA |
| Gary Mitchum | University of South Florida |
| Jessica Hausman | JPL/Caltech/NASA |

## Introduction

Maintenance and improvements to the fidelity of the TOPEX/Poseidon, Jason-1 and Jason-2/OSTM (TPJAOS) Sea Surface Height Climate Data Record (SSH CDR) is a continuous effort through the research activities of the Ocean Surface Topography Science Team (OSTST). As further advancements and/or re-calibrations are made to any of the correction parameters or models, the TPJAOS product is recalculated with the most accurate algorithms sanctioned by the OSTST. Notification and details of revisions to the TPJAOS will be provided and announced by the Physical Oceanography Distributed Active Archive Center (PODAAC) and displayed at this site http://podaac.jpl.nasa.gov/Integrated_Multi-Mission_Ocean_AltimeterData. Users will be notified of revisions to ensure they are consistently up to date.

Since the last quarterly release of TPJAOS v3.2, a number of algorithm revision/improvements along with the integration of Jason-3 data prompted the release of a revised version 4.0. In summary the following revisions were incorporated in the development of TPJAOS version 4.0, which spans through Jason-3 cycle 025 at this writing:

- GSFC itrf2014/dpod2014-based orbit replacing std1504 for all missions
- Extending SSH time series with Jason-3 altimetry
- DTU15 MSS reference
- Cross-track gradient correction based on DTU15 MSS derived cross-track slopes
- Revised inter-mission bias estimates

The following sections of this report detail these and other revisions to the SSH record and any subsequent impacts to validation results and mean sea level estimates. Users are referred to the Version 1.0 and 2.0 handbooks (ftp://podaac.jpl.nasa.gov/allData/merged_alt/preview/L2/docs/) for algorithm specifications that have remained unchanged.

## 1.0 General Structure Characteristics

The MEaSURE's TPJAOS v4.0 sea surface height (SSH) anomaly product is a multi-mission data set comprised of TOPEX/Poseidon (T/P), Jason-1, OSTM (Jason-2), and Jason-3 altimeter data integrated to form a single SSH Climate Data Record (CDR). Altimeter data from the multi-mission Geophysical Data Records (GDRs) are interpolated to a common reference orbit facilitating direct time series analysis of the geo-referenced SSH. The baseline v4.0 file is comprised of 887 10-day repeat cycles:

| | | |
|---|---|---|
| Cycle | 1 – 355 | T/P (cycles 1 – 355) |
| | 356 – 582 | Jason-1 (cycles 13 -239) |
| | 583 – 865 | Jason-2 (cycles 1 – 283) |
| | 866 – 887 | Jason-3 (cycles 4 -25) |

As future Jason-3 cycles become available the direct access structure of the file allows new data to be appended. All inter-mission biases have been applied to provide a seamless transition throughout the current 24+ year record.

Each 10-day repeat cycle is comprised of 127 revolutions. Each revolution has 6745 along-track locations spanning the equatorial ascending node (Figure 1).

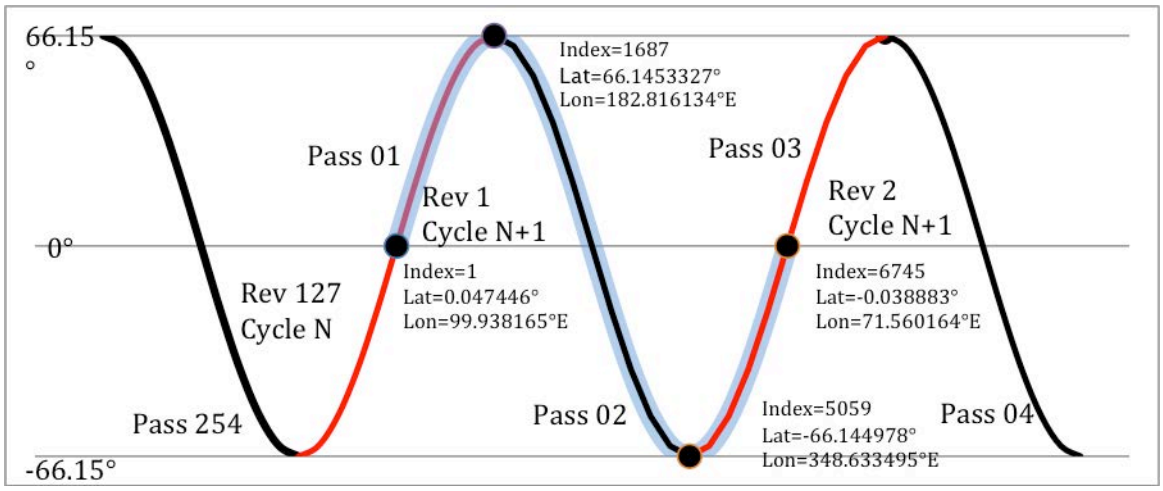


**Figure 1 : GDR convention of ascending odd numbered passes (solid red lines) and descending even numbered passes (solid black lines) total 254 passes/repeat cycle. The MEaSURE's product convention is based on 127-revolutions/repeat cycle. Revolution #1 is shown (blue shading overlay) with reference orbit lat/lon coordinates indicated for first and last geo-reference index, and for index at maximum and minimum latitude.**

Each SSH data record is a SSH time series at a specific geo-referenced location defined by revolution number and along-track index. A 3-dimensional directory (rev#, index, cycle) permits direct access of individual locations at specific times (i.e. temporal and spatial sub-sampling). Auxiliary files provide time, mean sea surface reference, terrain type, bathymetry, proximity to coast, and SSH quality assessments (flag word) at each geo-referenced location.

## 1.1 Geo-referenced 1Hz SSH

Construction of the 1Hz geo-referenced SSH is achieved by sampling the GDR high-rate SSH (10Hz for T/P and 20Hz for Jason-1 and OSTM) from contiguous 1Hz samples that align with the reference index location, and the time at the reference location derived from the GDR (Figure 2).

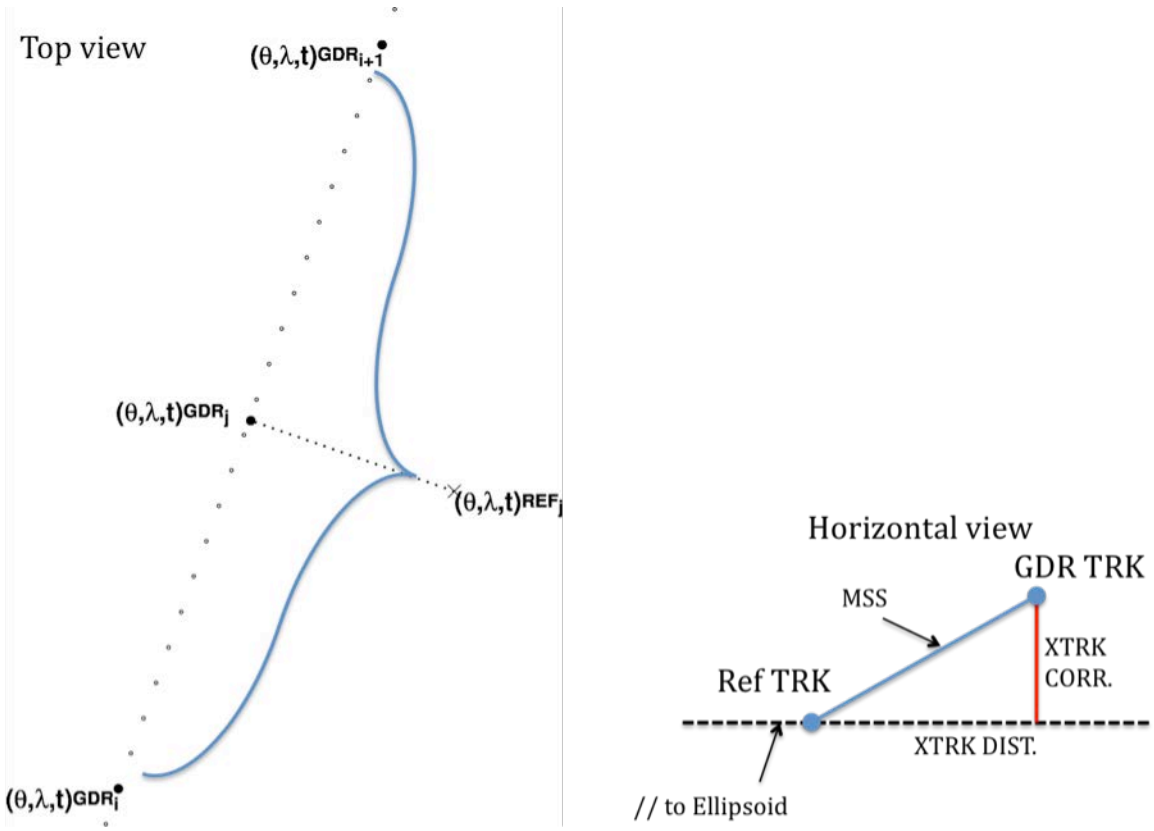


**Figure 2: 1Hz SSH constructed at reference orbit locations ($REF_j$) is achieved by re-sampling high-rate SSH from contiguous 1Hz GDR SSH ($GDR_i$ and $GDR_{i+1}$) evaluated at mid-point $GDR_j$.**

Satellites can deviate from the nominal orbit ground track by up to ± 1 km. To correct for this, a Mean Sea Surface [MSS] model can be used to effect a cross-track transformation between the along-track SSH and the corresponding SSH on the reference orbit. Towards this end, the normal projected onto the GDR groundtrack from the reference location provides the cross-track distance. The product of the cross-track distance and the local slope of the DTU15 MSS (Andersen et al., 2015) provide the cross-track gradient correction (Brenner et al, 1990) applied to account for local MSS gradients. The regression fit of the high-rate SSH is performed employing the GDR routine g1071 (TOPEX Ground System Science Algorithm Specification, 1991). Additional constraints require a minimum number of high-rate SSH (6 for T/P, and 16 for Jason-1, 2 and 3), and a minimum number of high-rate SSH on each side of the midpoint (2 for T/P and 7 for Jason-1, 2, and 3). The standard deviation of the high-rate residuals with respect to the resultant 1Hz average fit is computed and incorporated in the SSH quality assessment flag word (see Table 2).

## 1.2 Construction of the Corrected SSH Anomaly

$SSH_{uncorrected}$ = Orbit (GSFC itrf2014/dpod2014) – $Range\_ku_{corrected\ (net\_instrument\_corection\_ku)}$

$SSH_{corrected} = SSH_{uncorrected}$ - Dry Troposphere Delay

- Wet Troposphere Delay
- Solid Earth Tide
- Ocean Tide
- Ocean Load Tide
- Pole Tide
- Ionosphere Delay
- Sea State Bias (SSB) Delay
- Atmospheric Load (IB)
- Cross-track gradient
+ inter-mission bias

$SSH_{anomaly} = SSH_{corrected}$ - DTU15 mean sea surface

**Note**: The SSH anomalies are with respect to DTU15 MSS. The user can construct SSH anomalies with respect to a collinear mean reference by first adding back the DTU15 MSS, which is made available as a separate auxiliary file.

The GDR heritage for each mission:

- T/P MGDR_B (Benada, 1997)
- Jason-1 GDR_E (Picot et al., 2016)
- OSTM GDR_D (OSTM/Jason-2 products handbook, December 2011)
- Jason-3 GDR_D (_T cycles 1-21) (Jason-3 Products handbook, February 2016)

Origination of individual range and geophysical corrections applied to the SSH for each mission is detailed in table 1. Corrections employed that were directly obtained from GDR are identified by their parameter name as in handbook in bold italics. Many of the altimeter corrections present on the mission GDRs have been recomputed to take advantage of more recent and accurate models and to insure consistency across missions. The development

and implementation of replacement or revised correction parameters are explained in sections below.

**Table 1: Heritage of range and geophysical corrections applied to the SSH for each mission.**

| | TOPEX | Poseidon | Jason-1 | Jason-2 (OSTM) | Jason-3 |
|---|---|---|---|---|---|
| Orbit | GSFC<br><br>itrf2014(SLR) /dpod2014 (DORIS) | GSFC<br><br>itrf2014 (SLR) /dpod2014 (DORIS) | GSFC<br><br>itrf2014 (SLR) /dpod2014 (DORIS) | GSFC<br><br>itrf2014 (SLR) /dpod2014 (DORIS) | GSFC<br><br>itrf2014 (SLR) /dpod2014 (DORIS) |
| Range Ku | ***Net_Instr_R_ Corr_K***<br><br>Cg ***range correction NOT applied*** | ***Net_Instr_R_ Corr_K***<br><br>C***g range correction NOT applied*** | ***net_instr_corr_ range_ku*** | ***net_instr_corr_ range_ku*** | ***net_instr_corr_ range_ku*** |
| Dry Trop. | ECMWF Interim Re-analysis | ECMWF Interim Re-analysis | ECMWF operational ***model_dry_tropo_ corr*** | ECMWF operational ***model_dry_tropo_ corr*** | ECMWF operational ***model_dry_tropo_ corr*** |
| Wet Trop. | TMR enhanced replacement product (2015) | TMR enhanced replacement product (2015) | GDR_E JMR<br><br>***rad_wet_tropo_ corr*** | GDR_D AMR<br><br>***rad_wet_tropo_ corr*** | GDR_T AMR<br><br>***rad_wet_tropo_ corr*** |
| Ocean Tide ** | GOT4.8 | GOT4.8 | GOT4.10 | GOT4.10 | GOT4.10 |
| Ocean Load Tide | GOT4.8 | GOT4.8 | GOT4.10 | GOT4.10 | GOT4.10 |
| Pole Tide | Desai et al., 2015 | Desai et al., 2015 | Desai et al., 2015 | Desai et al., 2015 | Desai et al., 2015 |
| Solid Earth Tide | *Cartwright and Tayler* [1971] and *Cartwright and Edden* [1973] ***H_Set*** | *Cartwright and Tayler* [1971] and *Cartwright and Edden* [1973] ***H_Set*** | *Cartwright and Tayler* [1971] and *Cartwright and Edden* [1973] ***solid_earth_tide*** | *Cartwright and Tayler* [1971] and *Cartwright and Edden* [1973] ***solid_earth_tide*** | *Cartwright and Tayler* [1971] and *Cartwright and Edden* [1973] ***solid_earth_tide*** |
| Iono | Dual-frequency ***Iono_Corr (smoothed)*** | Doris/GIM ***Iono_Dor*** | Dual-frequency ***iono_corr_alt_ku (smoothed*** | Dual-frequency ***iono_corr_alt_ku (smoothed)*** | Dual-frequency ***iono_corr_alt_ku (smoothed)*** |

| | | | | | |
|---|---|---|---|---|---|
| Sea State Bias | Non-parametric collinear residuals (Tran, et. al , 2010) | Parametric BM4 crossover residuals (Gaspar et al 1994) ***EMB_Gaspar*** | Non-parametric collinear residuals (Tran et. al, 2012) ***sea_state_bias_ku*** | Non-parametric collinear residuals (Tran et al 2013) | Non-parametric collinear residuals (Tran et al 2016) |
| Atmos-pheric load | Dynamic Atmospheric Correction (DAC) | Dynamic Atmospheric Correction (DAC) | ECMWF operational + MOG2D hi-frequency ***inv_bar_corr + hf_fluctuations corr*** | ECMWF operational + MOG2D hi-frequency ***inv_bar_corr + hf_fluctuations corr*** | ECMWF operational + MOG2D hi-frequency ***inv_bar_corr + hf_fluctuations corr*** |
| Cross-Track gradient | DTU15 MSS | DTU15 MSS | DTU15 MSS | DTU15 MSS | DTU15 MSS |
| Inter-mission range bias | 8 mm (Alt A/ B) | 6 mm wrt TOPEX | -14.0 mm wrt TOPEX | -14.0 mm wrt TOPEX | 15.3 mm wrt TOPEX |

** Includes 18.6-yr long-period tide.

A SSH anomaly with respect to the DTU15 mean sea surface (Andersen, 2016) is computed if all correction fields are available (i.e. various conventions used throughout not set to default value). If one or more of the corrections applied are outside accepted nominal ranges, a quality assessment flag word bit is set to indicate the less than optimal quality. This rationale allows maximum retention of coastal and inland water observations that may otherwise be edited as "blunders" by open ocean standards. Table 2 lists the nominal ranges for each correction that with few exceptions follows the GDR handbook recommendations.

**Table 2: Nominal ranges for individual correction parameters. Quality flag word bit #6 (see SSH Quality Flag Word description below) is set if any single correction parameter is outside nominal range.**

| Correction parameter | Nominal range |
|---|---|
| Dry Troposphere | > -2600 mm and < -1900 mm |
| Wet Troposphere | ≥ -600 mm and < 0 mm |
| Ocean Tide | > -5 m and < + 5 m |
| Load Tide | > -150 mm and < +150 mm |
| Pole Tide | ≥ -100 mm and ≤ +100 mm |
| Solid Earth Tide | ≥ -1000 mm and ≤ +1000 mm |
| Sea State Bias | ≥ -600 mm and ≤ 0 mm |
| Altimeter derived wind speed | ≥ 0 m/s and < 25 m/s |
| Atmospheric load | ≥ -1000 mm and ≤ +1000 mm |

## 1.3 SSH Quality Flag Word

For each 1Hz geo-referenced SSH anomaly, a flag word is assigned to further assess the quality of the resultant SSH determination and provide the capability for tailored edit strategies for particular user applications.

Bit 0 : blank

Bit 1 : = 0 Dual-frequency altimeter measurement

= 1 Single frequency altimeter measurement

Bit 2 : = 0 depth ≥ 200 meters

= 1 depth < 200 meters

Bit 3 : = 0 proximity to land ≥ 50 km

= 1 proximity to land < 50 km

Bit 4 : = 0 Sigma H of fit < 15 cm (< 20 cm for Poseidon-1)

= 1 Sigma H of fit ≥ 15 cm (≥ 20 cm for Poseidon-1)

Bit 5 : = 0 high rate SSH sampled from two contiguous 1Hz data observations

= 1 high rate SSH sampled from single 1Hz observation

Bit 6 : = 0 all SSH corrections within nominal range

= 1 one or more of SSH corrections outside nominal range

Bit 7 : = 0 Cross Track Distance < 1.0 km.

= 1 Cross Track Distance ≥ 1.0 km.

Bit 8 : = 0 Cross Track Slope < 10 cm/km.

= 1 Cross Track Slope ≥ 10 cm/km.

Bit 9 : = 0 Significant Wave Height < 8 m and > 0 m(Ku band)

= 1 Significant Wave Height ≥ 8 m or = 0 m(Ku band)

Bit 10 : = 0 Sea ice not detected

= 1 Sea ice detected

Bit 11 : = 0 No rain contamination detected

= 1 Possible rain contamination detected.

Bit 12 : = 0 Sigma0 ≥ 6 db and ≤ 27 db (Ku band)

= 1 Sigma0 < 6 db or > 27 db (Ku band)

Bit 13 : = 0 Attitude (Att_Wvf) ≥ 0 and ≤ 0.3 degrees (T/P)

= 0 off_nadir_angle_ku_wvf ≥ -.09 deg$^2$ and ≤ +.09 deg$^2$

= 1 Attitude (Att_Wvf) < 0 or > 0.3 degrees (T/P)

= 1 off_nadir_angle_ku_wvf < -.09 deg$^2$ or > +.09 deg$^2$

Bit 14 : = 0 radiometer observation NOT suspect (tmr_bad set=0)

= 1 radiometer observation suspect (tmr_bad set > 0)

Bit 15 : = 0 GOT4.8 minus FES04 tide models differ by ≤ 2 cm.

= 1 GOT4.8 minus FES-4 tide models differ by > 2 cm.

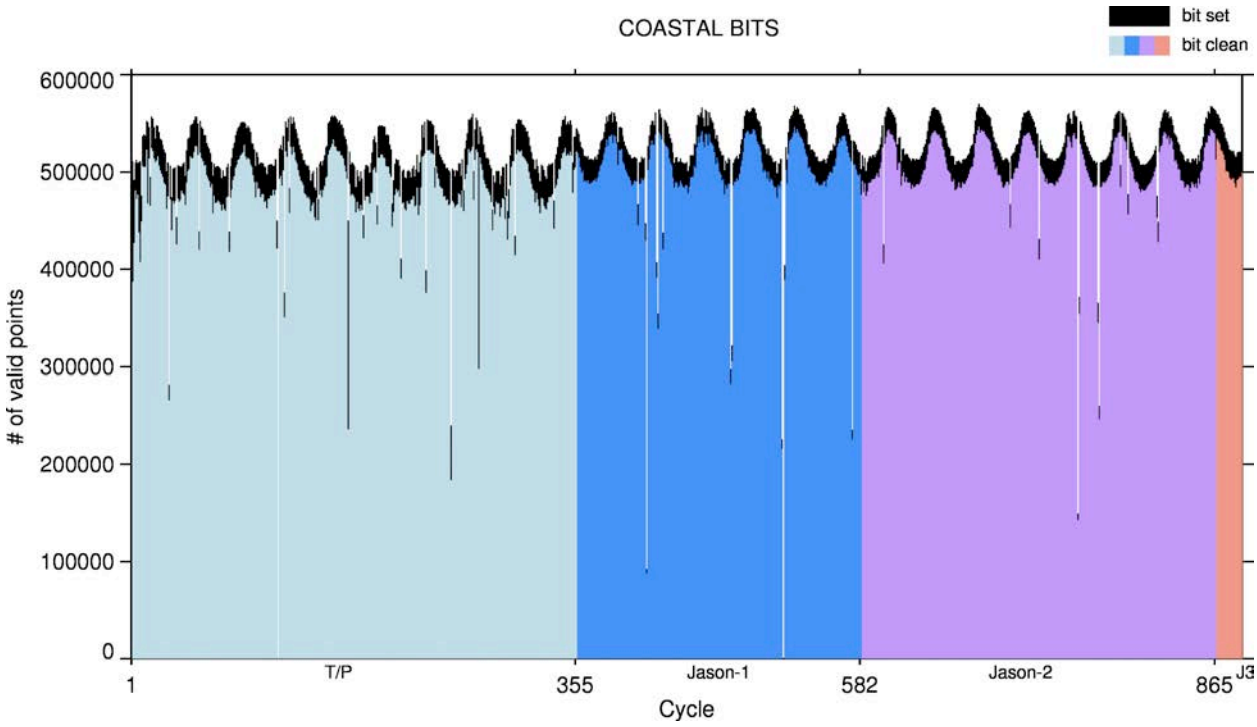


**Figure 3: Approximately 5% of valid (not set to default value of 32767) open ocean SSH anomalies are edited based on an edit strategy that requires bits 4-14 pass (i.e. equal 0). Bits 2,3, and 15 are not checked thus retaining coastal observations.**

# 2.0 Version 4.0 revisions to SSH computation

## 2.1 The GSFC replacement orbit height correction

Accurate orbit determination is central to the computation of the altimeter-derived surface elevation observation. The orbit defines the geocentric reference for the satellite altimeter sea surface measurement. Orbit accuracy and consistency are essential not only to the altimeter measurement accuracy across one mission, but also for the seamless transition between missions (Beckley, et. al, 2004). The analysis of altimeter data for TOPEX/Poseidon (TP), Jason-1 (J1) and Jason-2 (J2) requires that the orbits for all three missions be in a consistent reference frame, and calculated with the best possible standards to minimize error and maximize the data return from the time series, particularly with respect to the demanding application of consistently measuring global sea level change. This multi-mission altimetry time series can provide unprecedented insight into long-period ocean/atmosphere coupling needed for better understanding climate change. There are very demanding 1-cm radial orbit accuracy and cross-mission consistency objectives required to meet this goal (Cazenave et al., 2009, Ablain et al., 2009, Beckley et al., 2010). The orbit is also essential to calibrating the altimeter range, other altimeter corrections such as the sea state bias, and the inter-mission range bias. Such MEaSURE's altimeter bias corrections are based on the same orbits as are used for the geocentric height correction described in this section.

Insuring the highest accuracy and consistency of the satellite orbit is a critical component of the MEaSURE's task. Foremost is the application of improved GSFC replacement orbits that would tie multiple missions to a common well-defined geodetic reference frame (Beckley et al., 2007). Orbit testing at GSFC, has shown progressive improvement with increasingly refined POD modeling. Since 2009 GSFC has released five orbit series based on progressively improved POD standards: 1) the ITRF2005-based std0905, 2) the ITRF2008-based std1007 used previously in the MEaSURE's v1.0 product, 3) std1204 standards implemented in the MEaSURE's v2.0 product, 4) the ITRF2008-based std1504 standards implemented in the MEaSURE's v3.0 product, and 5) the ITRF2014-based dpod2014 standards implemented in the MEaSURE's v4.0 product.

The std0905 SLR/DORIS dynamic radial orbit accuracies have been accessed at 1.5 cm (Lemoine et al., 2010, Zelensky et al., 2010). Since then improvements to POD modeling standards have shown progressive improvement in orbit accuracy across all three missions. The latest standard, dpod2014, has upgraded to ITRF2014 from the ITRF2008 reference frame of the previous std1504 standard. The standard uses ITRF2014 for the SLR complements, and a specially tuned DORIS complement, dpod2014, produced by the IDS Combination Center led by Guilhem Moreaux (Toulouse, France). For convenience in this document we designate these SLR+DORIS-based orbits to be "dpod2014". Otherwise, dpod2014 orbits offer the same modeling as found with std1504. Table 3 outlines all the models and updates used in the dpod2014 standards. Several realizations of ITRF2014 SLR and DORIS complements have become available over the last year and have been evaluated at GSFC (Table 4). POD tests across the TOPEX, Jason-1, Jason-2 missions and including Jason-3 have identified the DORIS (DPOD2014.v04) + SLR (ITRF2014-IGN augmented)

combination to be superior in performance and completeness over the others. This combination of complements was selected to define the new dpod2014 standards. An example of the many tests used in making this selection is shown for Jason-3 (Table 5).

Although both GRACE-derived and the recent SLR/DORIS derived TVG models significantly improve the orbits from about 2005, the GRACE-derived TVG models do not accurately project back into the TOPEX era (Zelensky et al, 2012, Rudenko et al., 2014). To ensure consistency across missions we use TVG models derived from SLR/DORIS data. The dpod2014 gravity field includes 5x5 degree/order modeling of changes in the geopotential using stacked solutions of linear, annual, semi-annual terms derived from weekly 5x5 normal equations from 21 SLR/DORIS satellites, estimated over two spans: 1993-2002, 2003-2014 (Lemoine et al., 2014 update).

SLR/DORIS precise orbits were generated for the entire T/P, Jason-1, Jason-2 (or OSTM: (Ocean Surface Topography Mission), and Jason-3 mission time series based on the most recent dpod2014 POD standards. POD tests of the latest dpod2014 standards show improvement in the T/P, Jason-1, Jason-2, and Jason-3 orbits over the previous std1504 series (Table 6). Figure 4a illustrates the dpod2014 orbit improvement relative to std1504 using SLR residual data, and Figure 4b using independent Crossover data. These revisions to the precise orbit provide the geodetic consistency requirement necessary to tie T/P, Jason-1, OSTM, and Jason-3.

| **Table 3. GSFC POD Model Standards winter 2017: dpod2014 (changes from std1504 in red) GEODYN version: 1507** | |
|---|---|
| **Reference frame and displacement of reference points** | |
| SLR | ITRF2014 (Altamimi et al., 2016) augmented with 36 SLRF2008 stations transformed to ITRF2014; ILRS April 2014 data handling |
| DORIS | ITRF2014 (DPOD2014.v04) (Moreaux et al, 2016) |
| Earth tide | IERS2003 |
| Ocean loading | GOT4.10 all stations |
| Atmosphere loading | none |
| CoM | GOT4.7 tidal variations, annual SLR-derived (Ries 2013) |
| EOP | IERS Bulletin A daily (consistent with ITRF2008); Diurnal and semi-diurnal variations in polar motion and UT1 due to ocean tides. |
| Precession / Nutation | IAU2000 |

| | | | |
|---|---|---|---|
| **Gravity** | | | |
| Static | stack5x5_nom9k8 5x5 weekly normal equations from 21 SLR/DORIS satellites estimated over two spans: 1993-2002, 2003-2014; GOCO2S (from 6x6) | | |
| Time varying | stack5x5_nom9k8 linear, annual, semi-annual estimates from stacked 5x5 SLR+DORIS 21-years of weekly normal equations for two spans as above + 6x20 annual terms from GRACE, IERS2010 C21/S21, estimate C31/S21 per arc | | |
| Atmospheric | ECMWF, 50x50@6hrs | | |
| Tides | GOT4.10 50x50 (ocean); IERS2003 (Earth) | | |
| **Satellite Surface Forces and attitude** | | | |
| Albedo /IR | Knocke et al. (1988) | | |
| Atmospheric drag | MSIS86 | | |
| Radiation pressure | **TOPEX** | **Jason-1** | **Jason-2** |
| | tuned 8-panel | 10-panel | Jason-1 10-panel |
| Radiation scale coeff. | $C_R$ = 1.0 | $C_R$ = 0.916 (tuned) | $C_R$ = 0.945 (tuned) |
| Attitude | nominal: yaw model<br>off-nominal: quaternions | Quaternions<br>measured sapa | Quaternions<br>measured sapa |
| **Tracking data and parameterization** | | | |
| Tracking data | SLR/DORIS (Jason1 DORIS corrected for SAA) | | |
| Troposphere Refraction | SLR: Mendez-Pavlis; DORIS: VMF1 | | |
| Parameterization | Drag/8 hrs + opr along & cross-track /12 hrs (TP 24 hrs)+ DORIS time bias /arc; 10-day arc dynamic solution | | |
| DORIS modeling | DORIS beacon frequency bias modeling; beacon phase center | | |
| **Antenna reference** | **TOPEX** | **Jason-1** | **Jason-2** |
| Satellite CoM | table | corrected table | table |

| | | | |
|---|---|---|---|
| SLR | LRA model | re-tuned | tuned |
| DORIS | pre-launch | pre-launch | tuned |
| **SLR/DORIS weight** | 10-cm / 2-mm/s | 10-cm / 3-mm/s; down-weight 14 SAA stations | 10-cm / 2-mm/s |

**Table 4. DORIS / SLR complements and POD tests**

| **DORIS** | **Description / Number stations (4-char id)** |
|---|---|
| dpod2008 | DPOD2008_v15 / 189 (v14 +11 new sites) |
| itrf2014 | ITRF2014 (IGN) / 160 |
| dtrf2014 | DTRF2014 (DGFI) / 153 |
| itrf2014 augment | ITRF2014 (IGN)+DPOD2008 / 192 |
| dpod2014 | DPOD2014_v04 / 195 |
| **SLR** | **Description / Number stations (4-char id)** |
| slrf2008 | SLRF2008 (150928) / 168 |
| itrf2014 | ITRF2014 (IGN) / 137 |
| dtrf2014 | DTRF2014 (DGFI) / 97 |
| itrf2014 augment | ITRF2014 (IGN)+SLRF2008 / 173 |
| **DORIS+SLR Tests** | **Description (DORIS + SLR)** |
| itrf2008 | dpod2008 + slrf2008 |
| itrf2014 | itrf2014 + itrf2014 |
| dtrf2014 | dtrf2014 + dtrf2014 |
| itrf2014 augment | itrf2014_aug + itrf2014_aug |

| | |
|---|---|
| dpod2014 | dpod2014 + itrf2014_aug |

**Table 5. Jason-3 POD TRF2014 evaluation summary**

| Satellite | Test (std1504) DORIS+SLR POD | Total stations | | Average RMS residuals | | |
|---|---|---|---|---|---|---|
| | | DORIS | SLR | DORIS** (mm/s) | SLR (cm) | Xover* (cm) |
| **Jason-3** | itrf2008 | 53 | 34 | 0.4012 | 0.937 | 5.322 |
| | dpod2014 | 58 | 34 | 0.3997 | 0.851 | 5.318 |
| *160217 –* | itrf2014.aug | 55 | 34 | 0.4009 | 0.862 | 5.321 |
| *161121* | itrf2014 | 43 | 29 | 0.3927 | 0.825 | 5.322 |
| *(cycles 1-28)* | dtrf2014 | 39 | 28 | 0.3906 | 0.822 | 5.333 |

* independent altimeter GDRT data cycles 1-19

** SAA DORIS stations down-weighted

**Table 6. Evaluation of dpod2014 SLR/DORIS orbit performance for TP, J1, J2, and J3**

| Mission | orbit | average RMS residuals | | |
|---|---|---|---|---|
| | | DORIS (mm/s) | SLR (cm) | Xover * (cm) |
| TP cycles 1-446 | std1504 | 0.4948 | 1.554 | 5.611 |
| Sep 1992 – Oct 2004 | dpod2014 | 0.4948 | 1.579 | 5.598 |
| | | | | |
| J1 cycles 1-259 | std1504 | 0.3668 | 0.741 | 5.506 |
| | dpod2014 | 0.3668 | 0.749 | 5.509 |

| | | | | |
|---|---|---|---|---|
| Jan 2002 – Jan 2009 | | | | |
| | | | | |
| J2 cycles 1-303<br>Jul 2008 – Sep 2016 | std1504 | 0.3812 | 0.878 | 5.314 |
| | dpod2014 | 0.3791 | 0.819 | 5.311 |
| | | | | |
| J3 cycles 1-28<br>(xovers cycles 1-19)<br>Feb 2016 – Nov 2016 | std1504 | 0.4012 | 0.937 | 5.322 |
| | dpod2014 | 0.3997 | 0.851 | 5.318 |
| * altimeter crossover data are independent | | | | |

The stability and accuracy of the orbit time series is affected by errors in the force models, terrestrial reference frame (TRF), and errors in the tracking data and measurement models. The pre-std1007 std0905 SLR/DORIS dynamic orbits are believed accurate to 1.5 to 2 cm for TP, and closer to 1-cm for Jason-1/2 (Lemoine et al., 2010, Zelensky et al., 2010). The post-std0905 standards offer further improvement to orbit accuracy.

Fig 4c shows global orbit difference rates over water between std1504-dpod2014 are neglibible over the three missions. The tiny radial orbit rates shown in Fig 4c are consistent with the IGN ITRF2014 -> ITRF2008 Z-rate transformation parameter of -0.1 mm/year. Even on the regional scale, the radial rates are still very small, and do not exceed ±0.1 mm/year over the three missions (Fig 4d). Although the RMS radial differences are also small at the 1-2 mm level, they are seen to rapidly begin to increase following 2010 (Fig 4e). The increase is due to degredation in the std1504 orbits, and which is mostly due to increasing station position error when extrapolated past the ITRF2008 station solution span of 2009.0, as illustrated in Fig 4a. The evaluation between the std1504 and dpod2014 orbits indicates the impact of the differences between the ITRF2008 and ITRF2014-based stations on the orbits is small, but will increase over time.

Several topics are under investigation to further improve the current dpod2014 orbits. For example it has been shown errors in modeling of the mean pole especially after 2010, and calculation of pole tide lead to radial rate errors of order ±0.25 mm/yr (King and Watson, 2014). The impact of such errors and improved modeling of the mean pole are under investigation at GSFC.

Error in modeling the time variable gravity can produce systematic orbit error having annual, semi-annual and linear rate signatures. Although the problem of orbit rate error identification and mitigation still remains an open issue, it is believed that the JPL GPS reduced dynamic orbits are much less sensitive to dynamic error than other orbits (Bertiger et al., 2014). Using the Jason-2 JPL GPS RLSE14a/RLSE16a (ITRF2008–based) reduced dynamic orbits (jpl14a/jpl16a) as a reference we see the mean radial differences

between either std1504 or dpod2014 which can impact global MSL rate estimates is negligible (Fig 4f). However Fig 4f also shows an annual signature increasing in amplitude after 2014. This could be due to extrapolation error of the TVG field past 2014 which is used for the GSFC orbits (Table 3). On a regional scale the rates do not exceed ±1.0 mm/year for either std1504 or dpod2014 orbits (Fig 4g, Fig 4h). TVG modeling improvement remains under investigation at GSFC.

The redistribution of continental water, atmospheric and oceanic mass in the Earth system causes displacements of the Center of Mass of the Earth ($CM_E$), which are termed variations in geocenter. Ries (2013) derived an annual model of geocenter variations from analysis of Lageos-1 and Lageos-2 data, which has been applied in the dpod2014 standards. It has been shown that SLR/DORIS – based orbits reflect the Terrestrial Reference Frame (TRF) rather than the instantaneous $CM_E$ origin and so it is important to correct such orbits for $CM_E$ motion (Melachroinos et al. 2012). The Ries (2013) model did not consider the effects of atmosphere loading deformation on the SLR station positions. Analysis has shown that although the Ries model better aligns the orbit with the instantaneous $CM_E$ origin, atmosphere loading should not be used in combination with $CM_E$ models, which did not consider atmosphere loading in their development (Zelensky et al., 2014). Investigation at GSFC has shown that a $CM_E$ model developed with Lageos-1/2 data and atmosphere loading further improves orbit centering over the Ries model (Zelensky et al., 2016). Atmosphere loading in itself also improves station modeling in addition. $CM_E$ model improvement remains under investigation at GSFC.

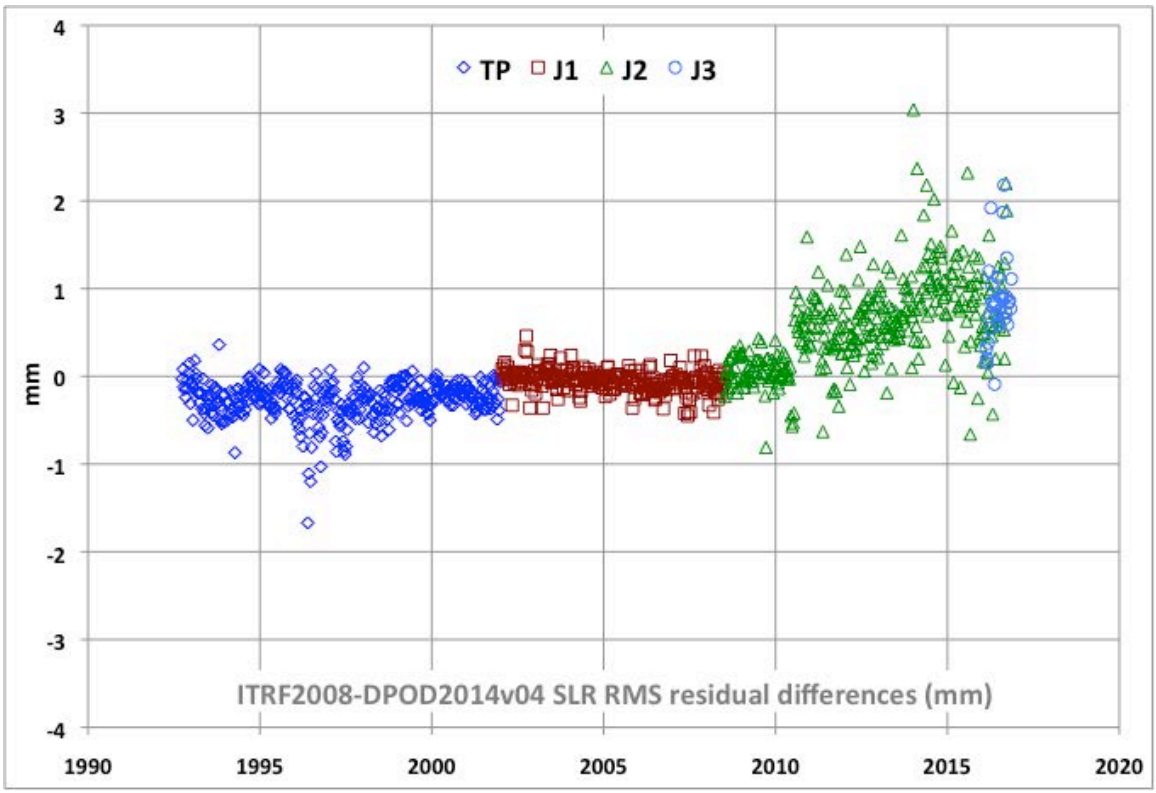


**Figure 4a: Dpod2014 radial orbit accuracy relative to std1504 using SLR data. Positive values indicate improvement derived from dpod2014.**

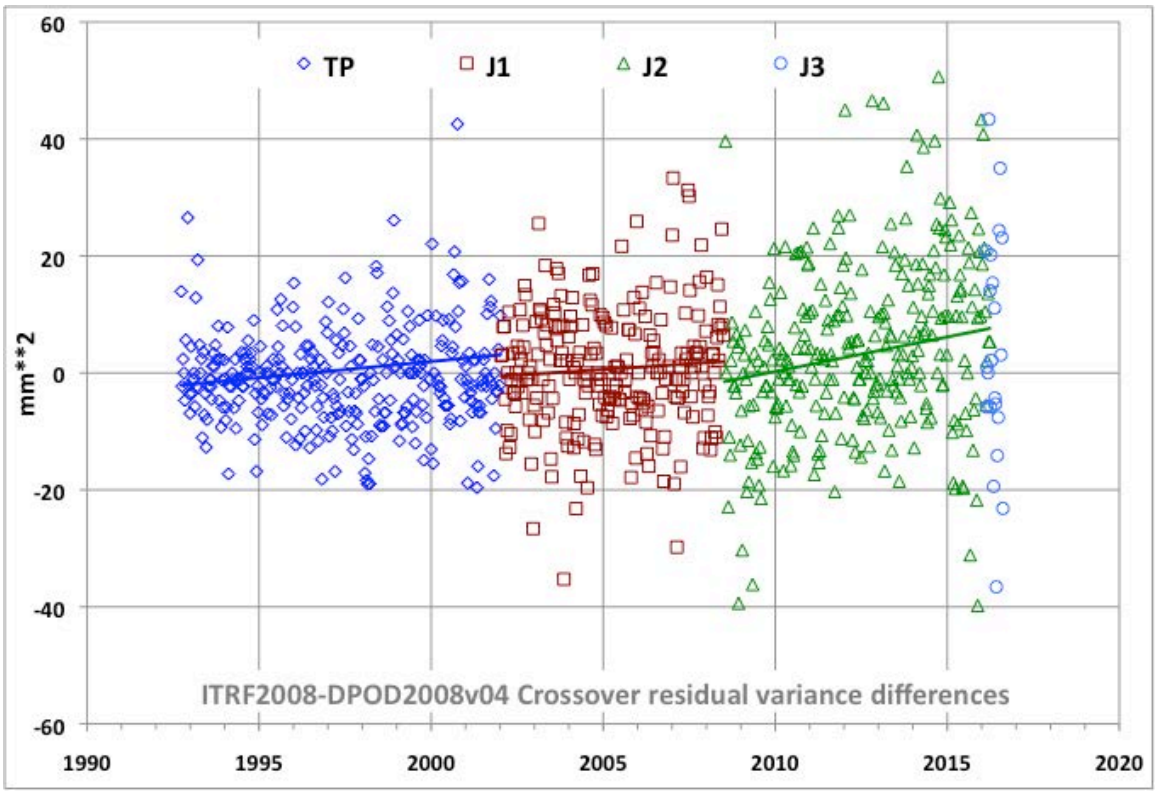


**Figure 4b: Dpod2014 radial orbit accuracy relative to std1504 using Crossover data. Positive values indicate improvement derived from dpod2014.**

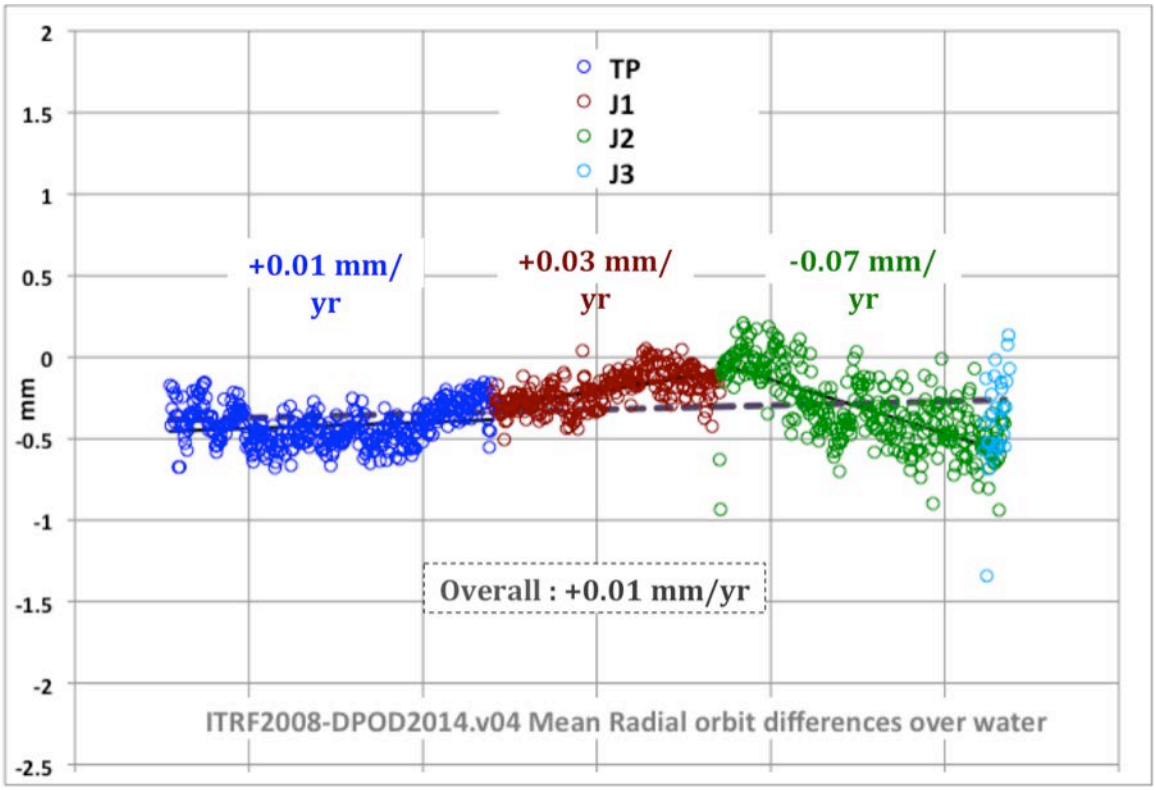


**Figure 4c: Mean radial std1504-dpod2014 orbit differences/cycle over water.**

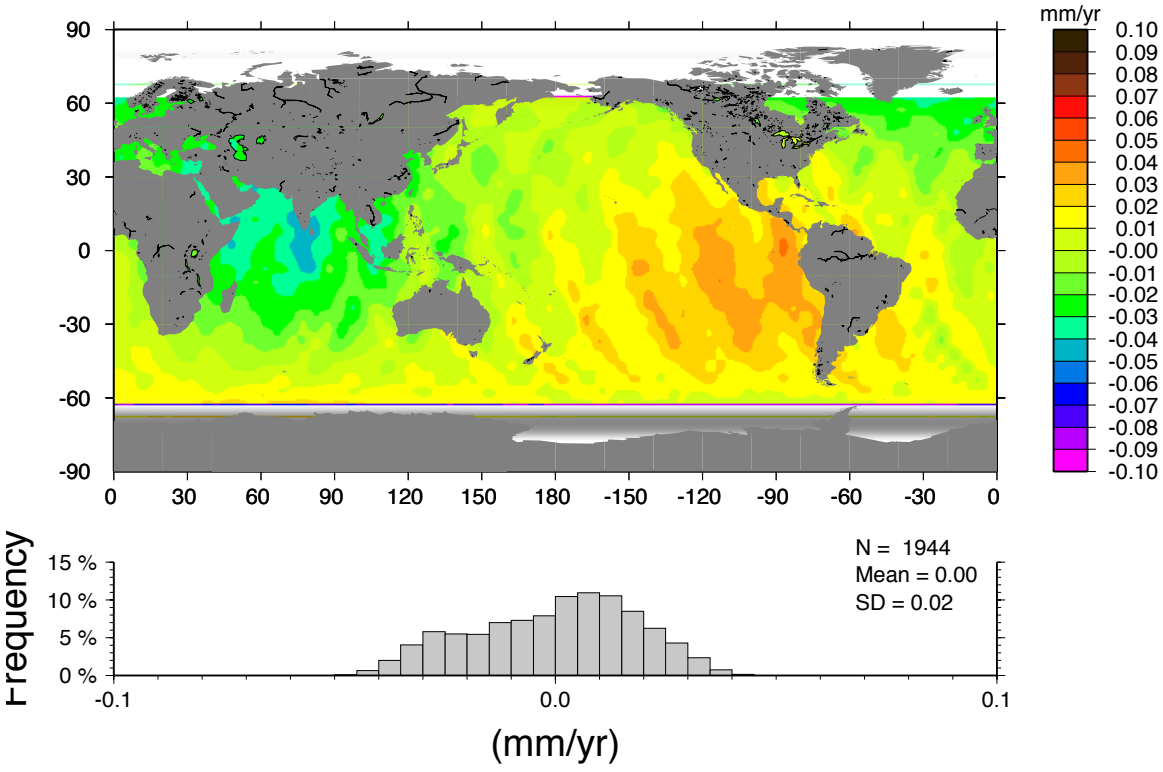


**Figure 4d: Std1504 – dpod2014 radial orbit difference linear rates (mm/y) estimated over September 1992 – September 2016 (across TOPEX, Jason-1, Jason-2, Jason-3). Mean rate over all water is near zero.**

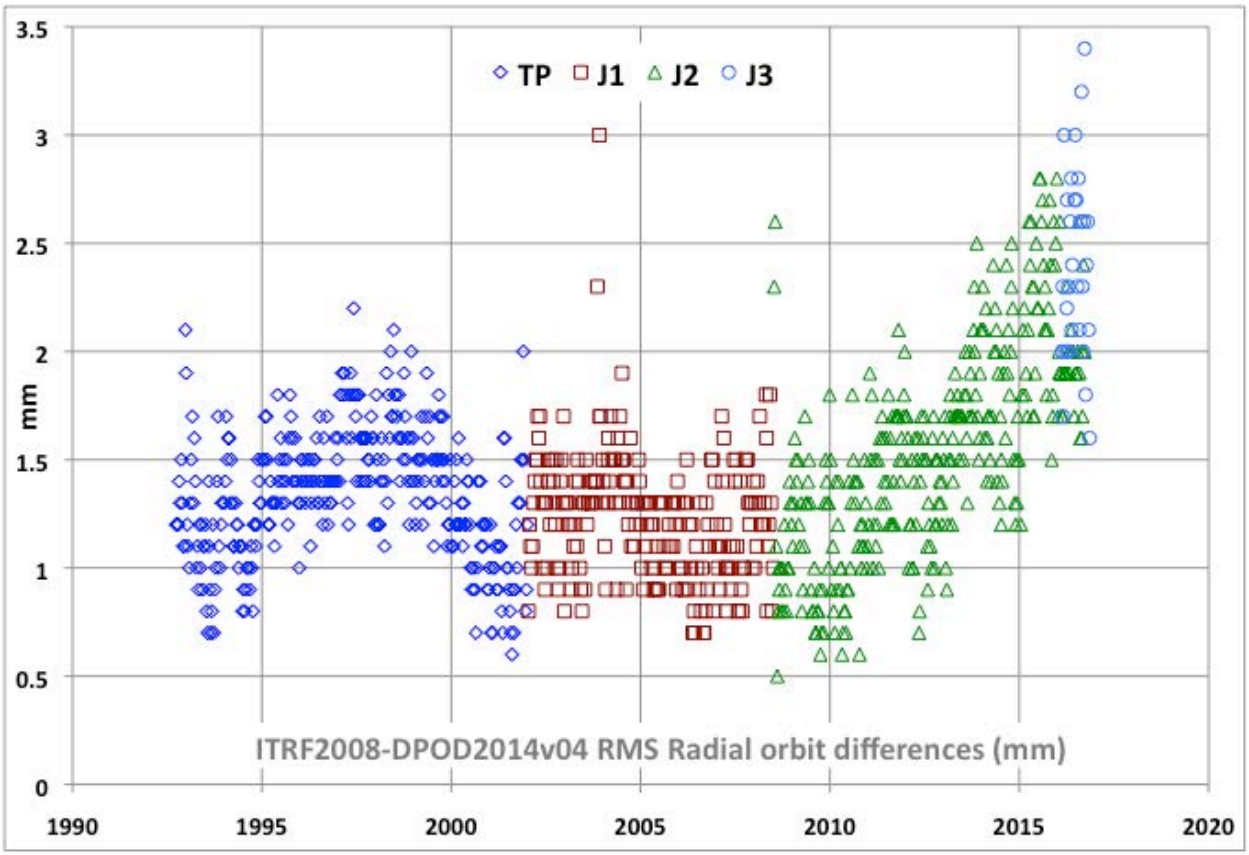


**Figure . RMS of radial std1504-dpod2014 orbit differences/cycle.**

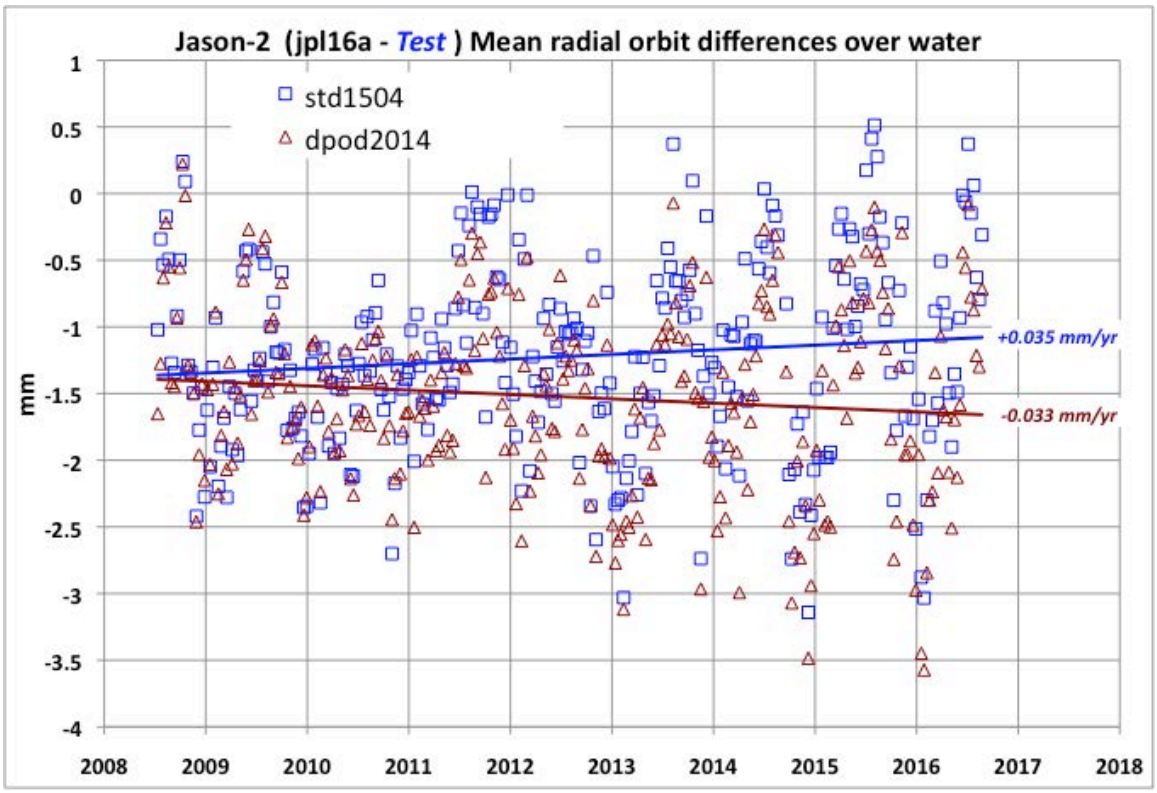


**Figure 4f: Jason-2 jpl16a - Test radial orbit differences over water July 2008 – August 2016 (cycles 1-300).**

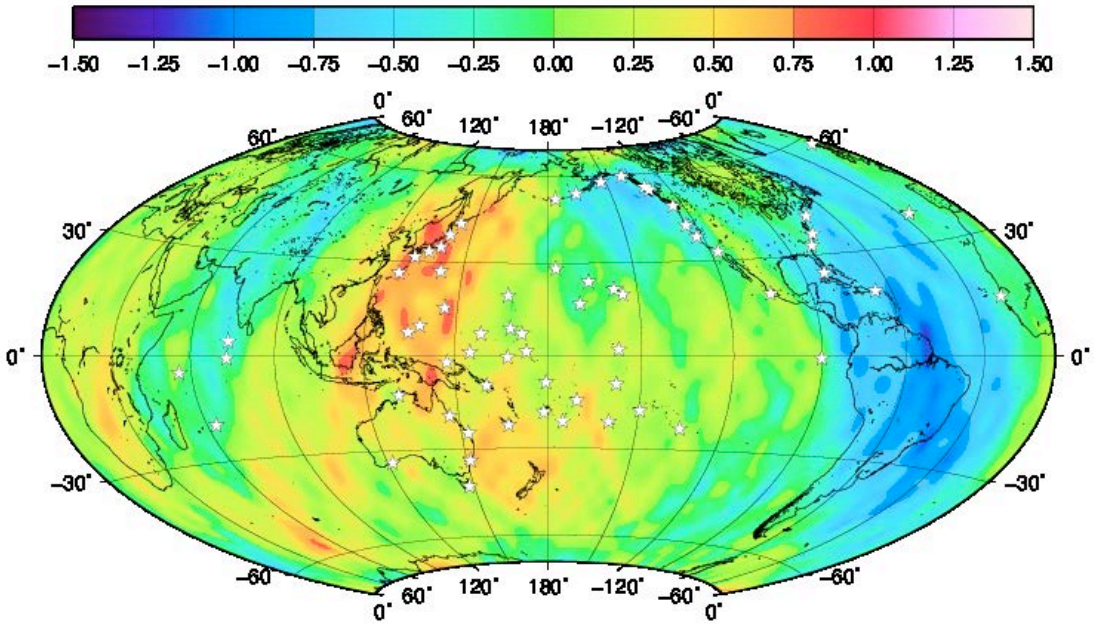


**Figure 4g: Jason-2 jpl14a – std1504 radial orbit difference linear rates (mm/y) estimated over July 2008 – August 2014 (cycles 1-225) after removing annual, semi-annual, and 118-day terms.**

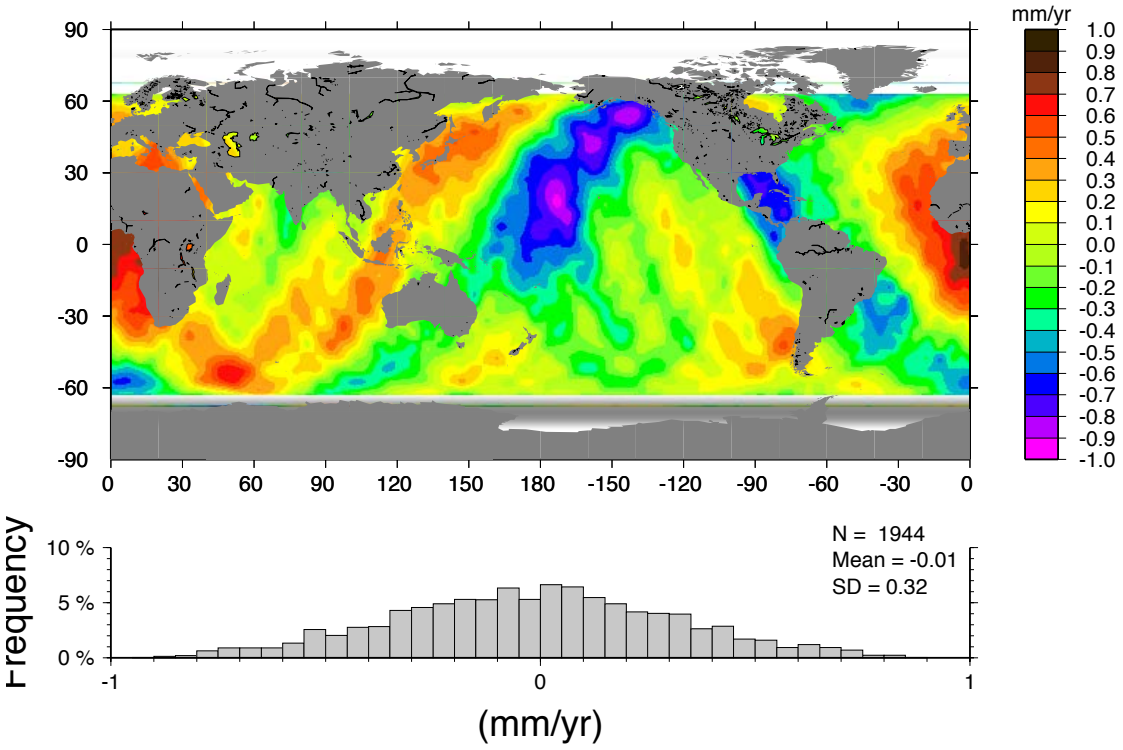


**Figure 4h: Jason-2 jpl16a – dpod2014 radial orbit difference linear rates (mm/y) estimated over July 2008 – August 2016 (cycles 1-300).**

**Re-calibrated Jason-1 Microwave Radiometer (JMR)**

Over the course of the Jason-1 mission several re-calibrations were performed to maintain and adhere to wet path delay (PD) stability/drift requirements (Brown, 2014). The most recent re-calibration to date is the end-of-mission climate quality calibration for the JMR (Brown, 2014) to be included in the GDR_E release. The end-of-mission re-calibration builds on previous calibrations, addresses remaining short term and long term residual calibration instability issues evident in the data (Figure 5), and implements revised algorithms brought up to Jason-2 GDR_D standards.

To stabilize the long-term calibration, an inter-satellite calibration approach was applied. This approach essentially transfers the long-term calibration from other stable externally calibrated satellite microwave radiometers to the altimeter radiometers. The calibration standard in this case was chosen to be the SSM/I TB fundamental climate data record (FCDR) (Kummerow et al., 2010).

In addition to the long-term trend, JMR also exhibited time variable changes in calibration instrument temperature dependency. The effect is to introduce transient 60-day variations, which cannot be easily detected using the TB references, but is very apparent when comparing the geophysical retrievals to other references. A process was developed to infer the TB instrument temperature dependence over a 120-day moving window from comparisons of the path delay to the ECMWF model and the AMR wind speed to the altimeter wind speed. This correction was applied along with the long-term drift. Finally, the JMR algorithms were updated to the Jason-2 GDR-D standard using the same processing software as is used for Jason-2 processing, but with coefficients specific to the JMR.

A drift correction has been applied to the final GDR_C calibration, which takes the form of a time variable scale and offset correction:

$$TB(ch,t)_{corrected} = TB(ch,t)_{uncorrected} - \Delta T_B(ch,t)$$

$$\Delta T_B(ch,t) = c_0(ch,t) + c_1(ch,t)TB(ch,t)_{uncorrected}$$

where the coefficients are derived by forcing agreement with the SSM/I Tb FCDR and on-Earth references (over the ocean (cold end) and over the Amazon rainforest (warm end)). The SSM/I FCDR was developed by Colorado State University (CSU) for NOAA and extends from 1987 to the present, covering the altimeter time period. The inter-satellite calibration provides a second independent reference (in addition to the natural reference method) and the demonstrated agreement between the two gives confidence in the observed long-term TB drift. Month-to-month calibration uncertainty is about 0.2°K (~2mm in PD).

Estimated trend error (Figure 6) can be computed as a function of record length:

- 2 mm/yr uncertainty for any 1 year
- < 1 mm/yr uncertainty for time spans greater than 2 years
- << 1 mm/yr for mission

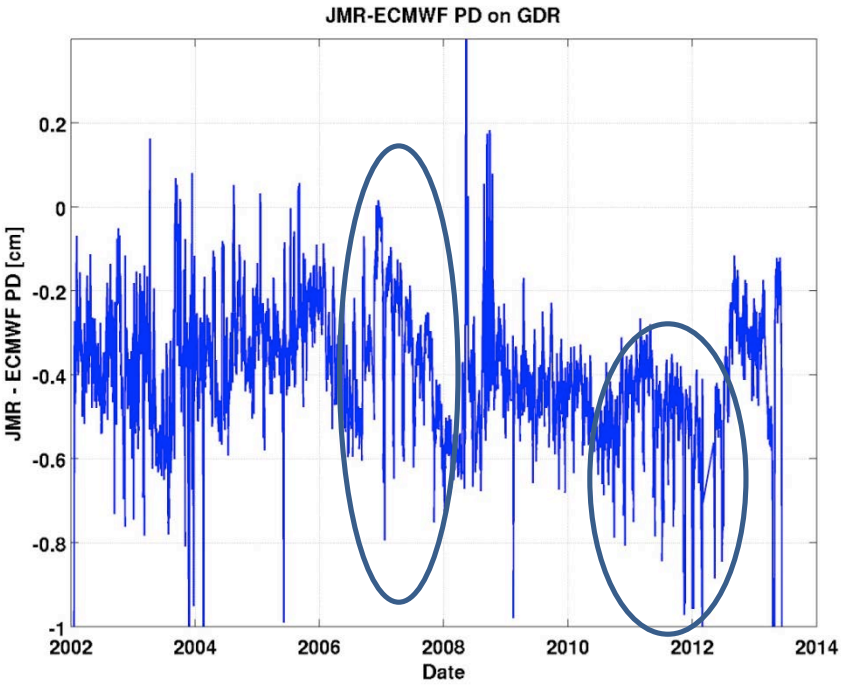


**Figure 5: JMR (GDR_C) minus ECMWF mean path delay differences detect times where further re-calibration is warranted.**

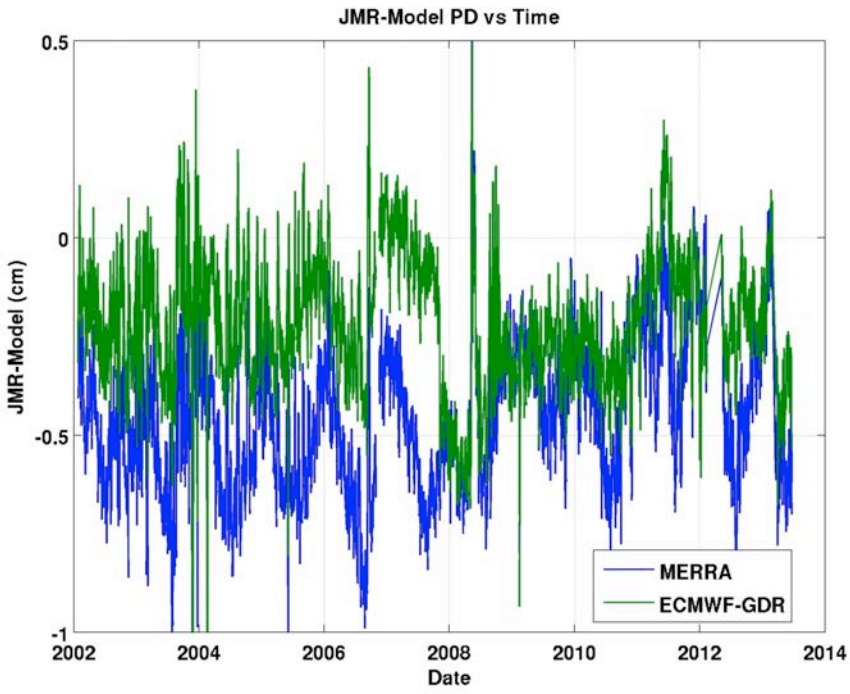


**Figure 6: Re-calibrated JMR versus MERRA and ECMWF model wet path delays suggest JMR drift rate less than 1mm/decade.**

Several JMR algorithms were updated to Jason-2 AMR standards:

- All-weather sigma-0 attenuation correction algorithm
- Consistent sea ice and rain flagging
- Near land path delay retrieval algorithm

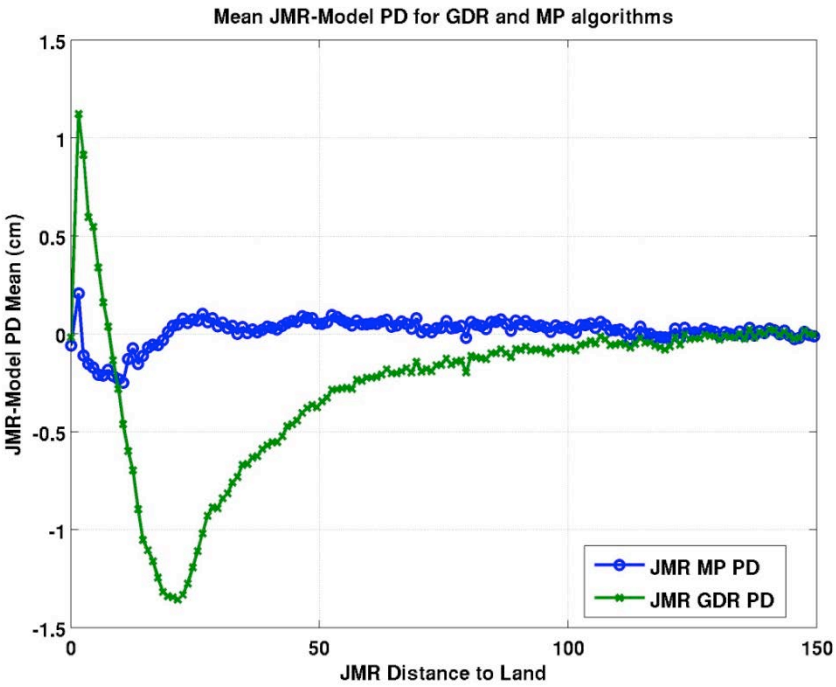


**Figure 7: Enhanced GDR_E JMR path delays recovered near land via mixed pixel (MP) algorithms provide improved accuracies in coastal areas.**

## 2.2 TOPEX Microwave Radiometer (TMR) Enhanced Wet Path Delays

The current GDR (MGDR_B) processing algorithm for TOPEX TMR uses a standard PD retrieval algorithm that underestimates path delay values near the coast due to land brightness temperature contamination. The application of a Mixed-Pixel algorithm on TOPEX TMR that has been has been successfully applied to the Advanced Microwave Radiometer (AMR) for Jason-2 and Jason-1 Microwave Radiometer (JMR) (Figure 7) to obtain coastal path delay values has been implemented. Algorithm performance on the TMR was compared with respect to the climate model MERRA (Figure 8) as well as JMR GDR processed PD values.

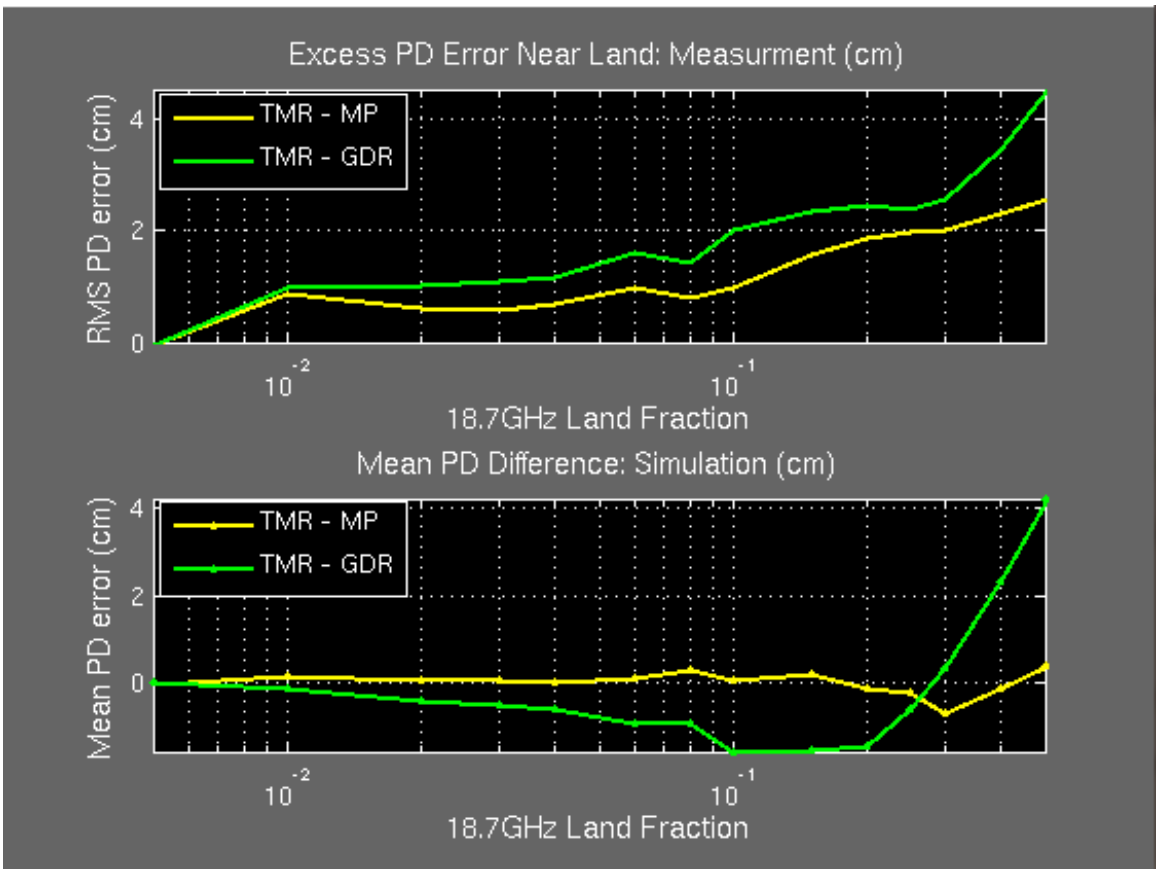


**Figure 8: The MP algorithm successfully compensates for land contamination. The figures above show the performance of the MP algorithm in terms of mean difference and RMS error with respect to MERRA. As observed, the GDR algorithm retrieved PDs have a characteristic dip as the land fraction increases. This is due to an increase in the 18GHz Tb that is not offset by increase in the higher frequency Tbs. The mixed pixel algorithm clearly has lower mean difference and RMS error compared to the GDR algorithm.**

## 2.3 Ocean Tide Corrections

The corrections for short-period (diurnal and faster) tides applied to TOPEX/Poseidon are based on GOT4.8, and those for Jason-1&2 are based on GOT4.10. The GOT4.8 model is derived from T/P altimetry only, while the GOT4.10 model is derived solely from Jason-1&2 altimetry. Model selection was based on accuracy assessments via comparisons to an improved bottom-pressure validation network (Stammer et al., 2015), and to the efficacy of the models to mitigate 59-day oscillations in altimetric global mean sea level (e.g., Masters et al., 2012). These are caused in part by errors in the S2 tide correction (the alias period of S2 is 59 d), as well as errors in anything correlated with solar forcing (radiation pressure, satellite thermal flexures, etc.), including the satellite center-of-gravity (Cg) correction. Unfortunately, it is now clear that at the level of 5-10 mm (roughly the amplitude of the 59-d oscillations in mean sea level), the T/P and Jason altimeters are inconsistent at the S2 frequency (Figure 9).

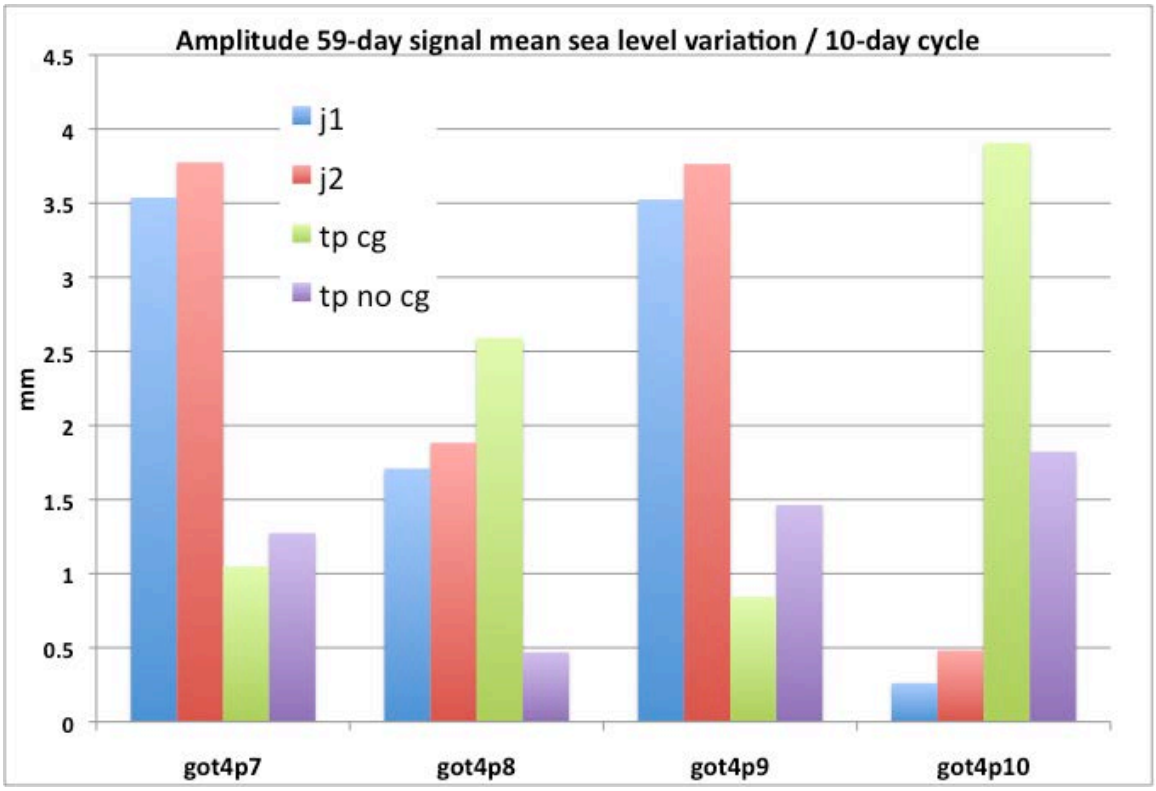


**Figure 9: The resultant amplitude of the 59-day signal that varies in T/P, Jason-1, and Jason-2 GMSL estimates with the application of ocean tide model, and the application of Cg to T/P altimetry.**

## 2.4 Pole Tide Correction

A revised pole tide correction has been developed (Desai et al., 2015) that replaces the earlier model contained in the T/P and Jason GDRs. The two primary revisions to the earlier model include 1) "upgrading to a self-consistent equilibrium model for the displacement of the ocean surface relative to the Earth's crust and explicitly modeling the load pole tide with respect to the CM", and 2) "that pole tide displacements for altimetry be computed from residual polar motion with respect to a drifting mean pole, with the rate determined from almost 80 years of observations (Argus and Gross, 2004)". The impact on global mean sea level estimates is negligible due to geographical cancellation of signal. Impact on regional sea level estimates range from ±0.25 mm/y (Figure 10).

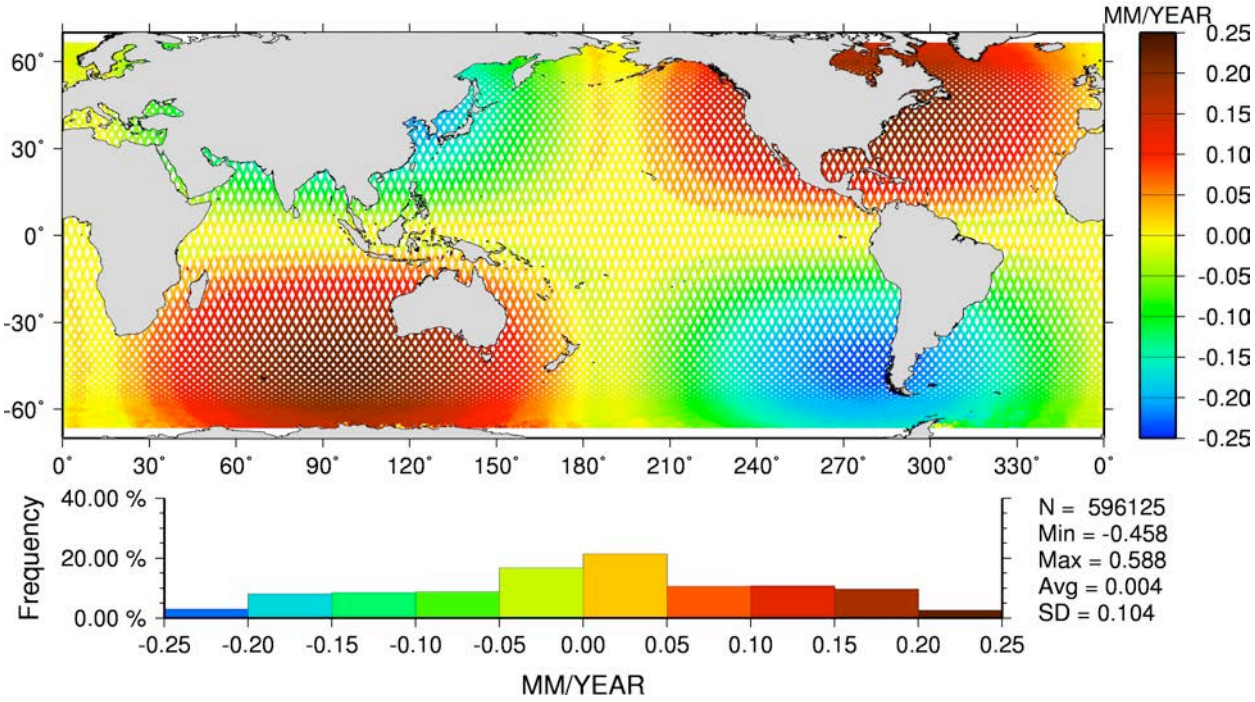


**Figure 10: Regional linear trends of pole tide differences between revised model (Desai, et al., 2015) and previous model contained in mission GDRs. The impact on regional sea level is at the level of +/- 0.25 mm/y.**

## 2.5 Mean Sea Surface

The DTU15 mean sea surface (Andersen, 2015.) replaces the DTU13 surface as the reference for the SSH anomalies, and for the generation of the cross-track gradient correction derived from the regional slopes at each geo-referenced location. Additional altimetry now derived from a 22+ year record and the inclusion of the Jason-1 geodetic mission data and CryoSat-2 data are incorporated in the generation of the DTU15 surface. Figure 11 shows DTU15 minus DTU13 mean sea surface differences evaluated at geo-referenced locations over ocean. Revised cross-track slopes based on the DTU15 MSS are shown in Figure 12. Cross-track slope differences evaluated at the geo-referenced locations over ocean between DTU15 and DTU13 are shown in Figure 13.

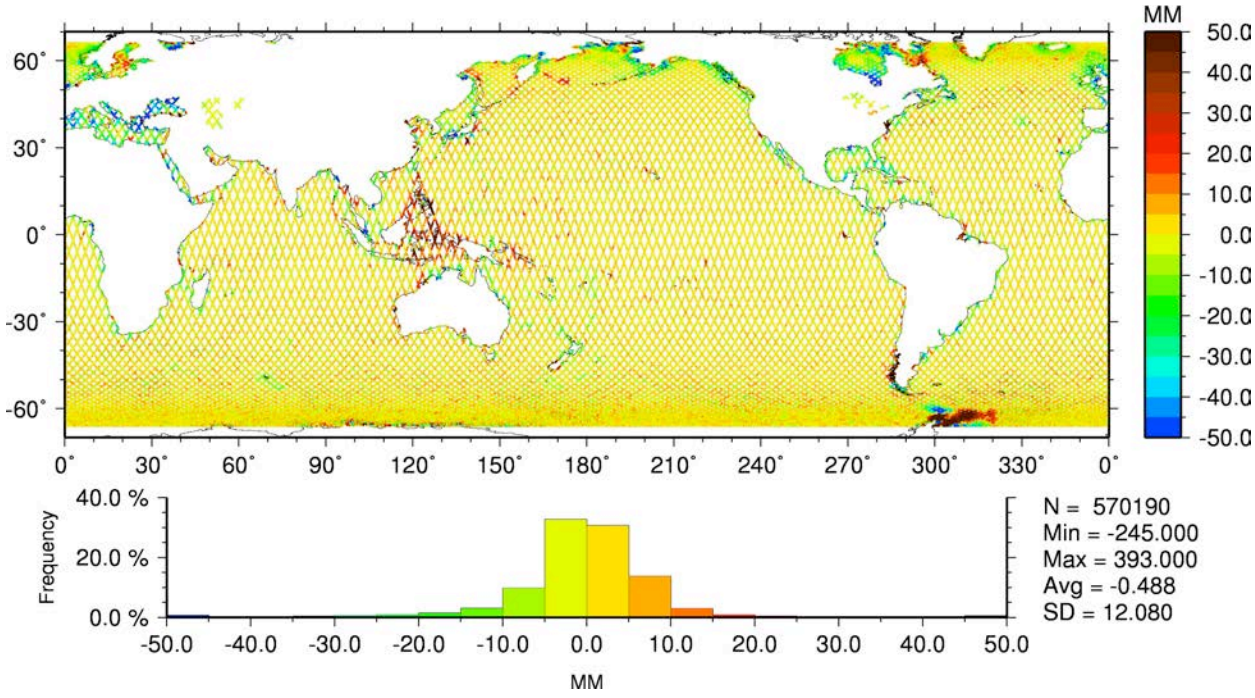


**Figure 11: DTU15 minus DTU13 mean sea surface elevation differences evaluated at geo-referenced locations over ocean.**

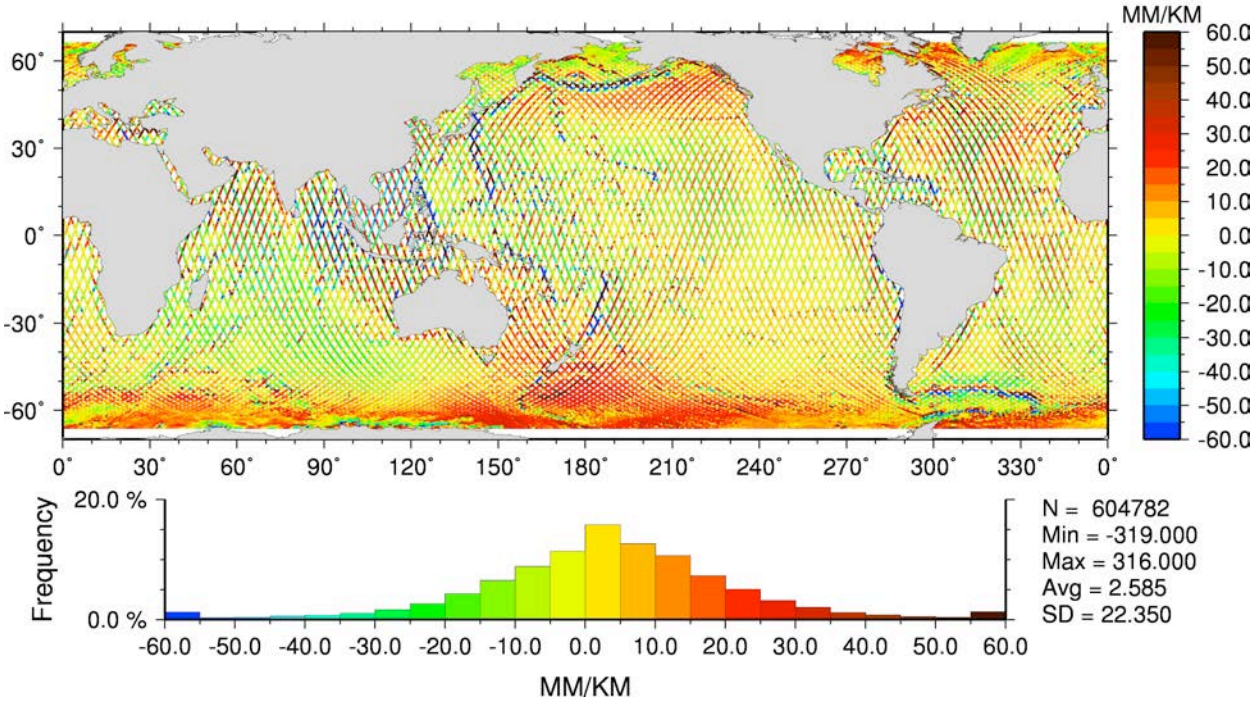


**Figure 12: Cross-track slopes evaluated at geo-referenced locations over ocean based on DTU15 MSS.**

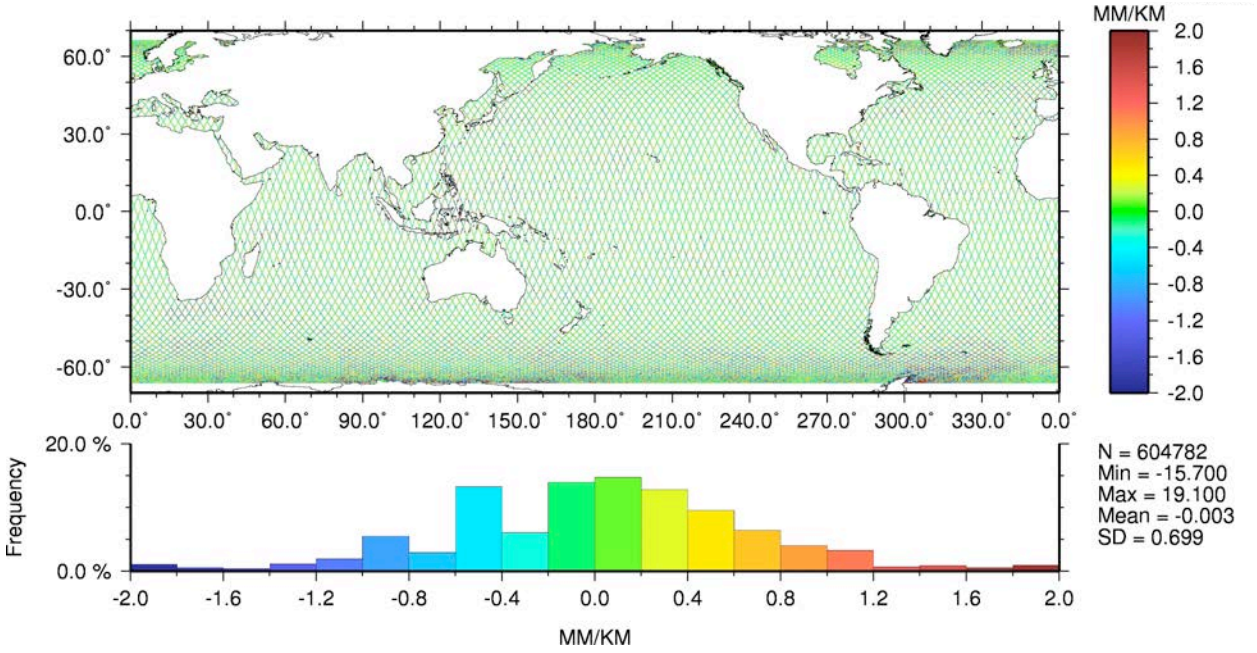


**Figure 13: Differences between cross-track slopes based on DTU15 versus DTU13.**

# 3.0 Inter-mission biases

## 3.1 Sea State Bias

In an effort to adhere to inter-mission consistency and provide a homogeneous SSH time series, the non-parametric (NP) sea state bias models that have evolved over time based on the works of Gaspar et al., 1998, 2002, Labroue et al., 2004, and most recently Tran et al., 2010&2012 have been employed to correct for sea state bias effects on the TOPEX, Jason-1&2 altimeters. Continuous improvements to these empirical based models has been due in part to improved POD strategies based on consistent geophysical modeling strategies and a single terrestrial reference frame adopted across all missions (Lemoine, et al, 2010), adoption of a consistent ground reprocessing strategy (4-parameter Maximum Likelihood Estimator (MLE4) re-tracking, Amarouche et al., 2004), improved atmospheric load corrections (Carrère and Lyard, 2003), and revised 2-parameter wind speed algorithms specifically tuned for TOPEX (Gourrion et al., 2002), and Jason-1 (Collard, 2004) altimeters. The specific SSB tables implemented for each mission are identified in Appendix II and can be obtained from AVISO.

A collaborative effort with Dr. Ngan Tran from CLS has produced non-parametric (NP) solutions for TOPEX (Side A and B) derived from collinear SSH residuals based on revised GSFC std0809 ITRF2005 (Eigen-GL04c) replacement orbits, and current correction algorithms outlined in Table 2 (Tran et al, 2010). Improved agreement between TOPEX and Jason-1 is realized with the application of the NP model as compared to results based on a revised parametric model derived from crossover residuals (Beckley, et al 2010). Comparison of the two models via SSH collinear differences (based on TPJAOS v1.0) shows an approximate +3mm Side A bias and -4.5mm Side B bias and an annual signature of 1mm in amplitude of the mean difference (Figure 17). Rectification of the approximate overall 7-

8 mm Side A/B bias is accomplished by comparing the altimeter derived SSH variations to the height variations from a near global network of tide gauges (see Tide Gauge Validation section below).

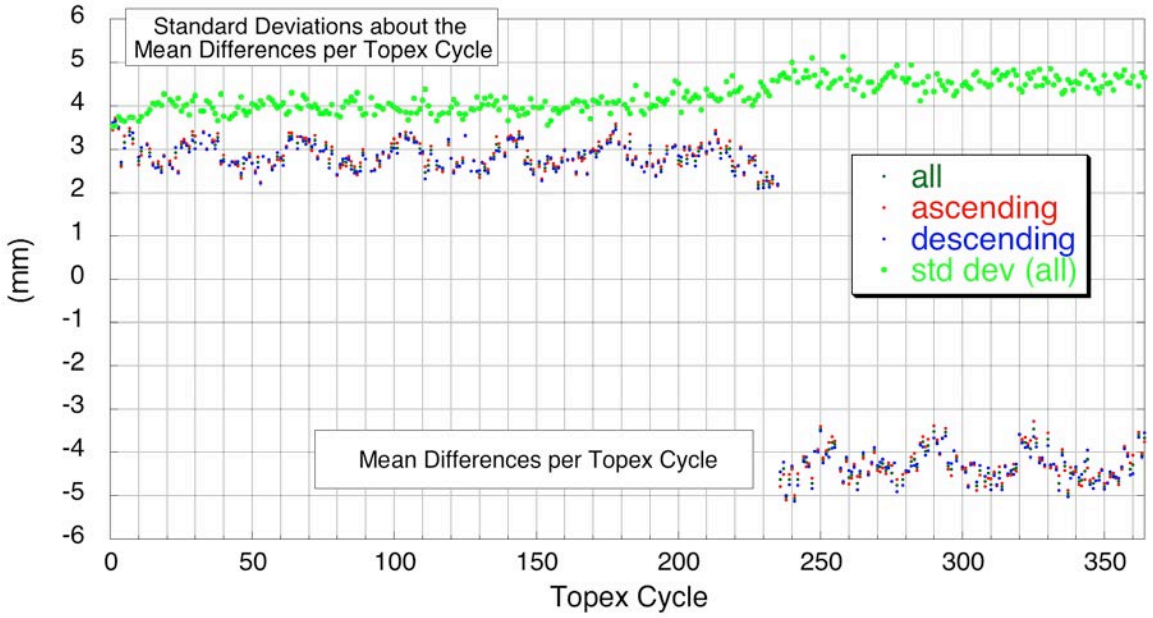


**Figure 14: Mean differences of sea surface height between heights based on parametric versus non-parametric sea state bias solutions reveals separate biases for TOPEX Side A (cycles 1-235) and for Side B (cycles 236-364).**

## 3.2 Jason-1, 2, & 3 Verification Phase Results

A critical component to providing credible mean sea level estimates from integrated multiple altimeter missions is the accurate determination of inter-mission biases. The verification campaigns during the roughly first 6 months of the Jason-1, 2, and 3 missions provided essential near-simultaneous altimeter observations that would enable the seamless transition from T/P to Jason-1 to Jason-2 to Jason-3.

Figures 15, 16, and 17 show the estimated global mean bias between TOPEX/Jason-1, Jason-1/Jason-2, and Jason-2/Jason-3 respectively derived from regional mean variations of the SSH collinear differences of the near-coincident measurements over the time period of the verification phase(s). All pertinent range and geophysical corrections are applied in order to identify and isolate any regional residual differences/errors attributed to any remaining unavoidable inter-mission inconsistencies. Each figure shows some expected regional variance in the estimate of the global mean bias estimate, though each estimate has a very normalized distribution of SSH mean residuals with a standard deviation not exceeding 2 mm.

Note the Jason-1/TOPEX inter-mission bias of 14.0 mm (Jason-1 SSH higher) shown in Figure 18 is with respect to an already adjusted TOPEX Side B with respect to Side A (see Figure 21). After several range correction omission errors were accounted for in the

Jason-1 GDR_E and Jason-2 GDR_D, the Jason-1/2 inter-mission bias is nearly zero (Figure 16), thus a bias of 14.0 mm is also applied to Jason-2 to align to the TOPEX reference datum. The Jason-2/Jason-3 bias shown in Figure 20 shows Jason-3 SSH to be 29.3 mm lower than Jason-2, this a bias of 15.3 mm is applied to Jason-3 to align to TOPEX.

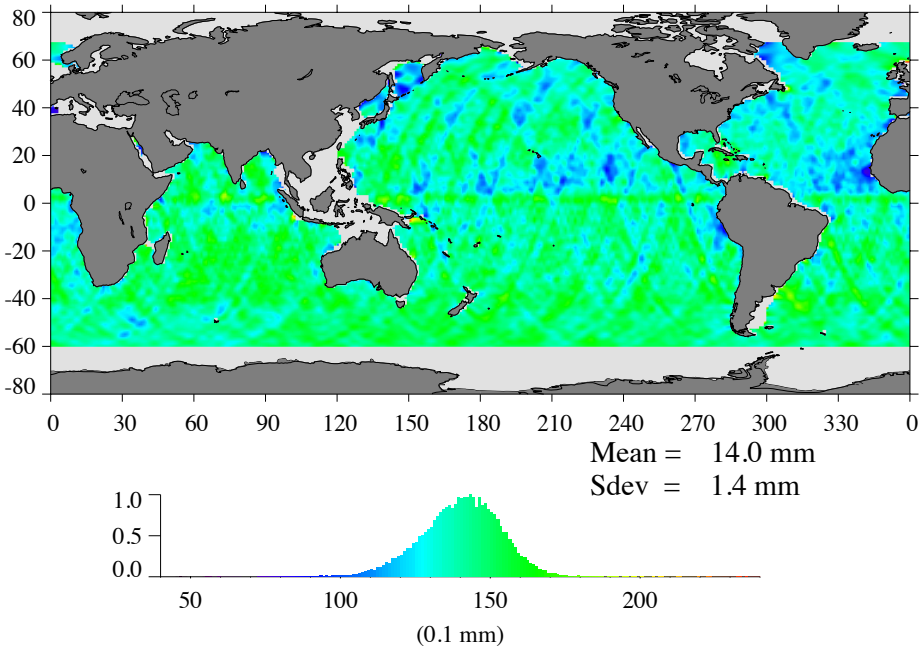


**Figure 15: Jason-1 minus TOPEX (adjusted Alt B) inter-mission bias is estimated from averaged SSH collinear residuals during the Jason-1 verification phase. Color scale is exactly +/- 1cm about estimated mean.**

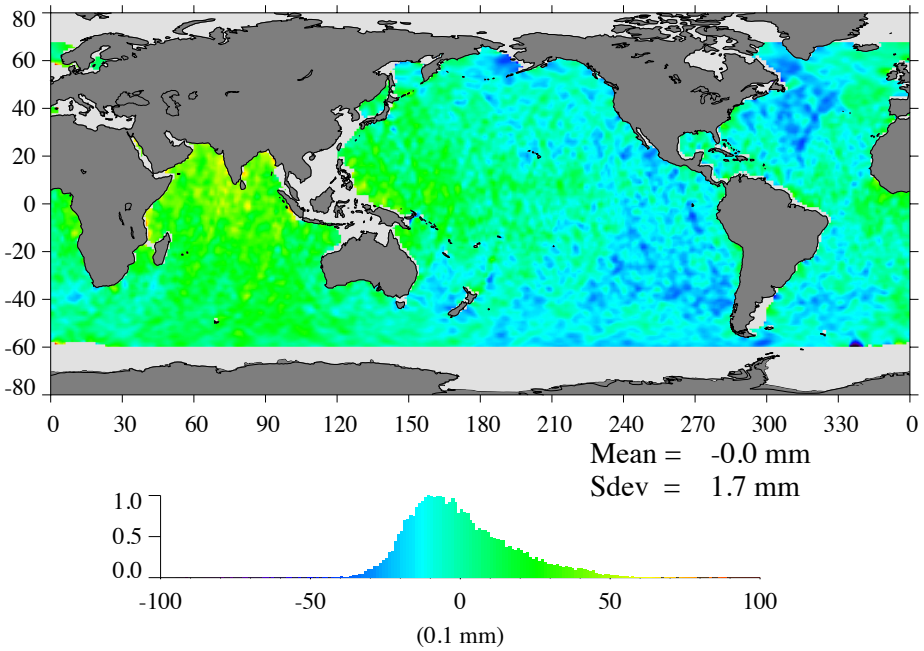


**Figure 16: Jason-2 minus Jason-1 inter-mission bias is estimated from averaged SSH collinear residuals during Jason-2 verification phase. Color scale is exactly +/- 1cm about estimated mean.**

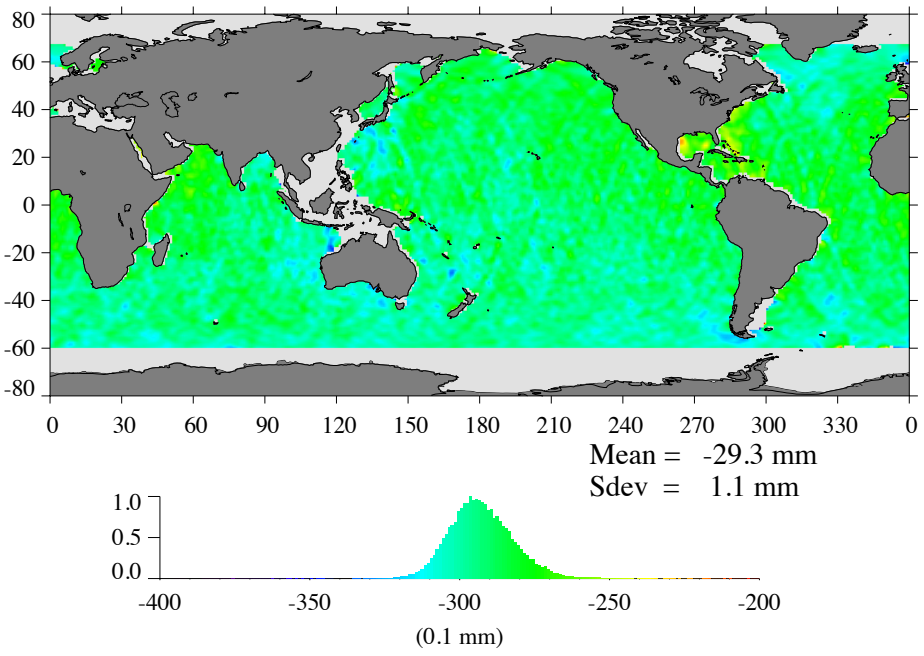


**Figure 17: Jason-3 minus Jason-2 inter-mission bias is estimated from averaged SSH collinear residuals during Jason-3 verification phase. Color scale is exactly +/- 1cm about estimated mean.**

## 3.3 Tide Gauge Validations

Validation procedures are regularly performed by Prof. Gary Mitchum by comparing altimeter derived SSH variations to height variations measured from a global network of tide gauges (Mitchum, 2000). From the beginning of the TOPEX/Poseidon (T/P) mission, methods to estimate altimeter drift from comparisons with the global tide gauge network have continuously evolved, (for example, as the SSH time series approached two decades, questions about the handling of long period tides, particularly the Msf and Mf components, were raised and we adapted our methods appropriately) first in a research mode with NASA funding (primarily the T/P and OST SWTs and later from MEaSUREs), and later becoming more general and operationally-oriented.

Validation results shown here are based on the current near-global network of 64 sites. Work is nearly completed that will expand the network to 84 sites, providing much needed information in the Southern Hemisphere (Figure 18). The largest uncertainty in estimated rates derived from the gauges arises from land motion at the sites. Vertical land motion corrections based on the latest ULR5 (University of La Rochelle Consortium) GPS velocity fields (Santamaría-Gómez et al., 2012, Wöppelmann et al., 2009) have been implemented.

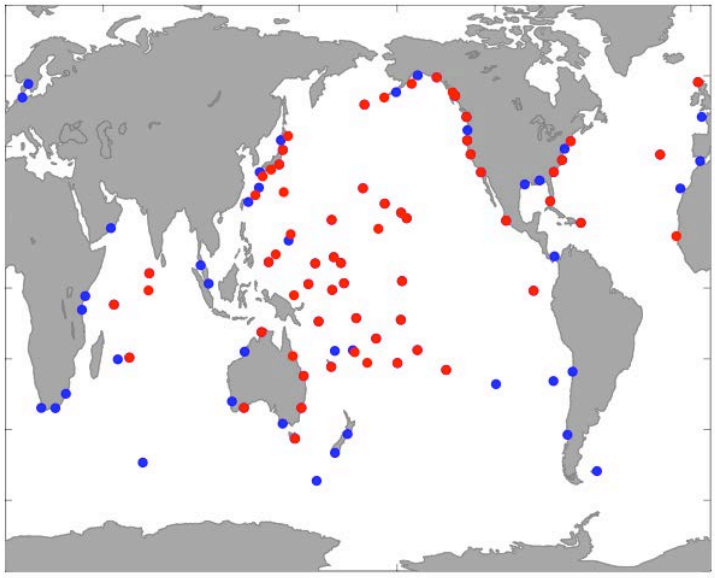

**Figure 18: Current network of 64-tide gauge sites (red dots); soon to be expanded to 84 sites (additional blue dots).**

The tide gauge validation analysis tools currently in place evaluates and monitors within-mission stability, and provides an assessment of inter-mission bias estimates (Nerem, et al., 2010, Leuliette and Scharoo, 2010, Beckley et al., 2010). As shown in figures 9 and 10 TOPEX/Jason-1 and Jason-1/Jason-2 inter-mission biases can be evaluated globally by direct SSH collinear differencing benefiting from the dedicated verification phases. The TOPEX Side A and Side B altimeters are treated as if separate missions as is noted in the independent evaluation of the sea state bias for each altimeter. There is no Side A/B

coincident overlapping data available thus we are reliant on the tide gauge network to estimate this particular "inter-mission" bias. Figure 19 shows an estimated Side A/B bias of 8 mm resultant to differences in mean variations to a common TOPEX reference. An adjustment to Poseidon-1 SSH is applied to account for an estimated bias of 6 mm (Poseidon-1 SSH lower with respect to TOPEX). The TOPEX/Poseidon-1 bias is estimated by computing the mean of T/P open-ocean collinear SSH residuals (figure 20). Note in earlier versions 1.0 and 2.0 the TOPEX/Poseidon-1 bias estimate was not applied to the Poseidon-1 SSH.

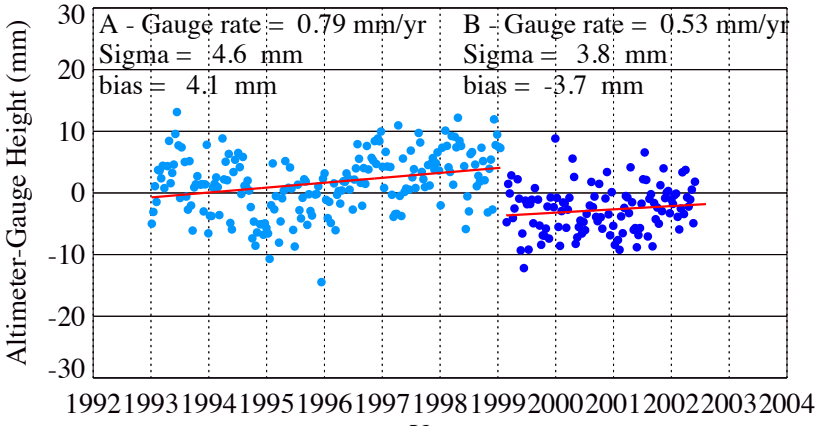


**Figure 19: Estimate of TOPEX Side A/B bias is derived from per cycle mean comparisons of altimeter SSH variations with height variations from 64-site tide gauge network.**

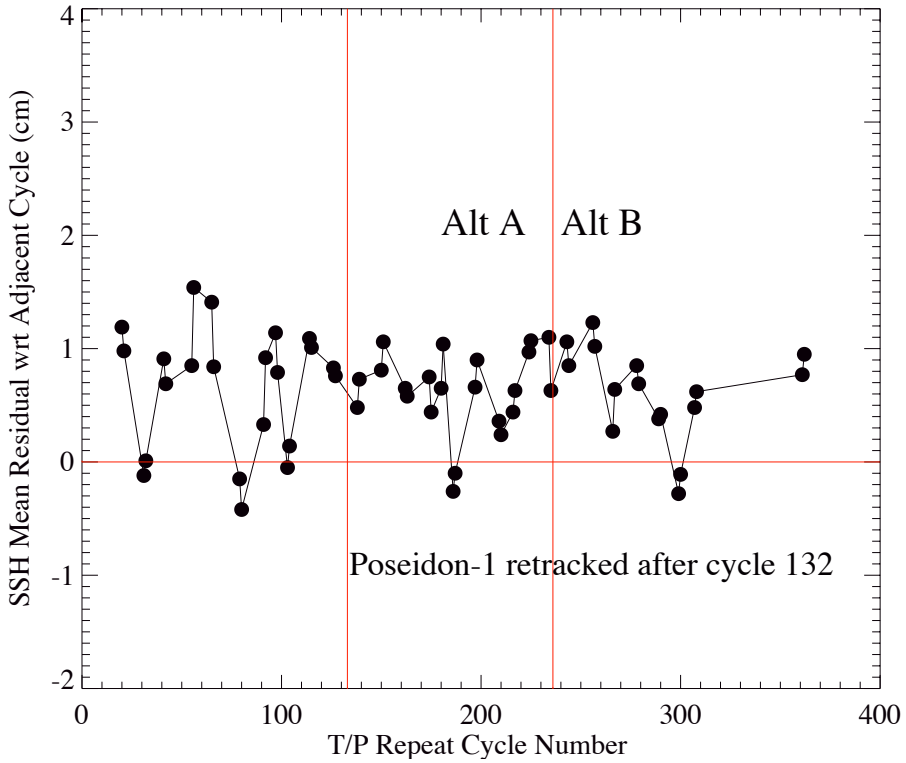


**Figure 20: Poseidon-1 bias with respect to TOPEX is estimated via mean collinear T/P SSH residuals. Before cycle 132, Poseidon-1 data is not retracked.**

To assess the inter-mission consistency and stability of the entire 24-year time series, the TOPEX A/B bias, and the adjustment biases to Jason-1 and Jason-2 that were derived from their verification campaign SSH collinear residuals are applied, and compared against a high-fidelity 64-site tide-gauge network as a "single mission" time series. These tide gauge comparisons provided in Figure 21 show per cycle mean differences to be predominantly within a ± 1.0 cm envelope, and to have an overall estimated "drift" rate of +0.14 mm/y with a standard deviation of the mean differences to the linear fit of 4.4 mm.

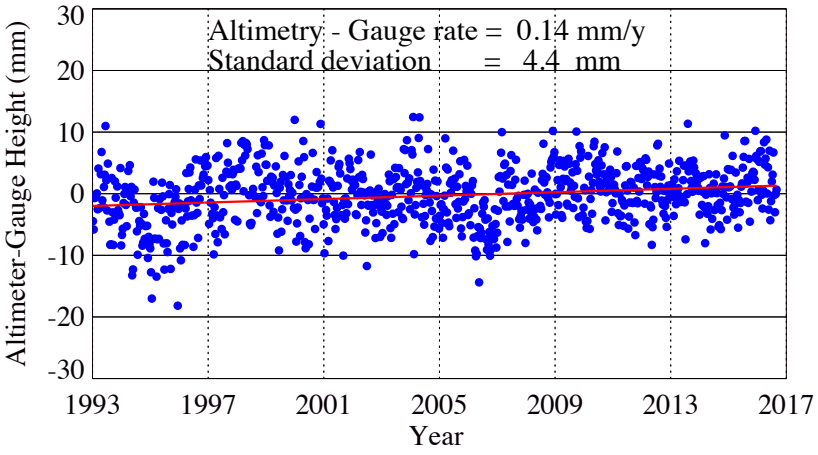


**Figure 21: Resultant per cycle comparisons of altimeter derived SSH variations with height variations from 64-site tide gauge network after application of inter-mission biases to form a single adjusted SSH Climate Data Record.**

# 4.0 Estimation of Global and Regional Mean Sea Level

Global and regional mean sea level variations derived from the TPJAOS v4.0 product are shown in Figures 22 through 24 below. Details of the derivation of the sea level estimates are provided in Beckley et al., 2007 and 2010. The examples below do have the glacial isostatic adjustment (GIA; Peltier 2009) applied; annual and semi-annual signals are intact in Figure 22, and have been removed in Figures 23 and 24. The edit strategy employed based on the quality flag word bits edited observations where any one of bits 1, 3-4, 9-14 where set to 1, or bits 7 and 8 both set to 1 (see Appendix). Observations where the terrain type is not equal to zero indicating non open-ocean are edited. The regional sea level trends though do include coastal SSH trend estimates.

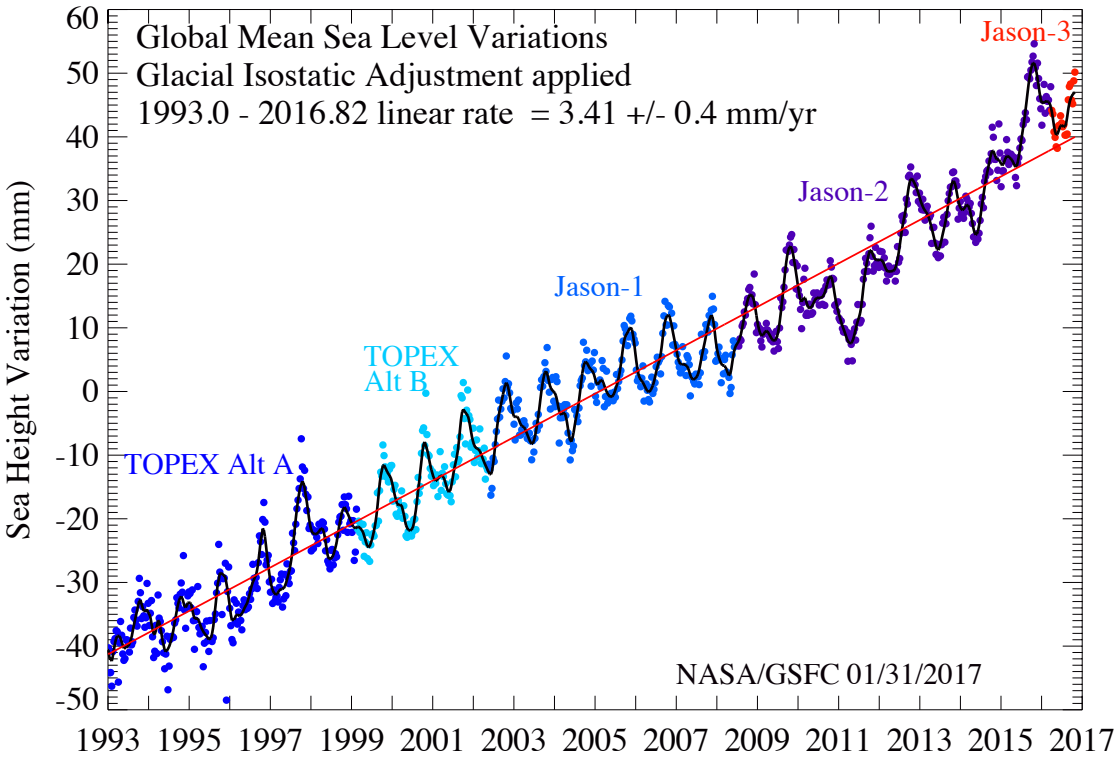


**Figure 22: Global mean sea level is estimated at 3.41 ± 0.4 mm/yr (GIA applied) based on SSH variations with respect to 20-year TOPEX/Jason mean profile. Sea surface heights are based on cycles 11-887 of TPJAOS v4.0 SSH anomaly product. Black line denotes SSH variation after application of 60-day Hanning filter.**

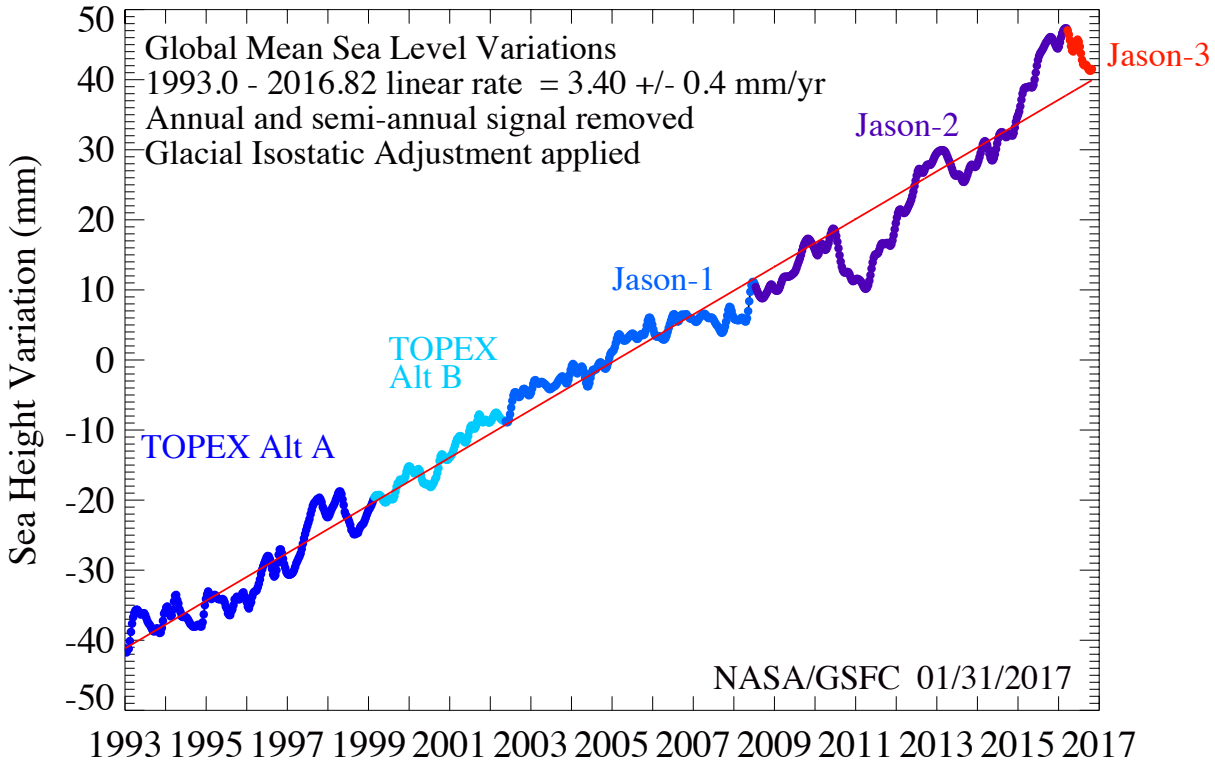


**Figure 23: Global mean sea level variations estimated as in Figure 22 with annual and semi-annual signal removed.**

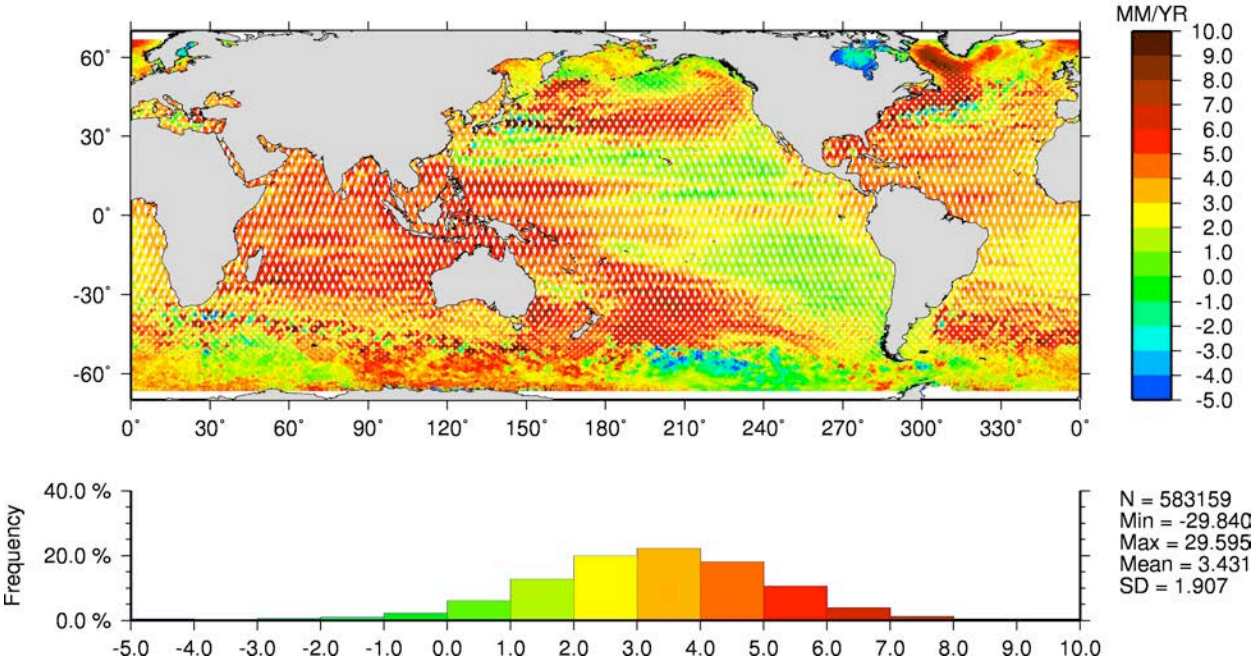


**Figure 24: Regional mean sea level variations (GIA applied, annual and semi-annual signal removed) at each geo-referenced location are based on cycles 11-887 of the TPJAOS v4.0 SSH anomaly product.**

# 5.0 References


Ablain, M., A. Cazenave, G. Valladeau, et al., A new assessment of the error budget of global mean sea level rate estimated by satellite altimetry over 1993–2008, Ocean Sci., 5, 193–201, 2009.

Altamimi, Z., P. Rebischung, L. Metivier, and C. Xavier (2016), ITRF2014: A new release of the International Terrestrial Reference Frame modeling nonlinear station motions, J. Geophys. Res. Solid Earth, 121, doi:10.1002/2016JB013098.

Amarouche L., P. Thibaut, O.Z. Zanife, P. Vincent, and N. Steunou. 2004. Improving the Jason-1 ground retracking to better account for attitude effects. *Marine Geodesy*, 27(1-2) :171-197.

Andersen, O. B., and P. Knudsen. 2009. DNSC08 mean sea surface and mean dynamic topography models. *J. Geophys. Res.,* 114, C11001, doi:10.1029/2008JC005179.

Andersen, O. B., 2010. The DTU10 Global Gravity field and Mean Sea Surface – improvements in the Arctic Ocean. Presented at the *2nd International Gravity Field Symposium*, 20-22 September 2010, Fairbanks, Alaska.

Andersen, O.B. et al., The DTU13 MSS (Mean Sea Surface) and MDT (Mean Dynamic Topography) from 20 Years of Satellite Altimetry, International Association of Geodesy Symposia, pp 1-10, 2015, doi:10.1007/1345_2015_182

Andersen, O. B., G. Piccioni, L. Stenseng, and P. Knudsen, The DTU15 Mean Sea Surface and Mean Dynamic Topography-focusing on Arctic issues and development., 2015 Ocean Surface Topography Science Team Meeting, Reston, VA, USA.

Beckley, B.D., N.P. Zelensky, S.B. Luthcke, and P.S. Callahan. 2004. Towards a seamless transition from TOPEX/Poseidon to Jason-1. *Marine Geodesy,* 27, 373-384.

Beckley, B.D., F.G. Lemoine, S.B. Luthcke, R.D. Ray, and N.P. Zelensky. 2007. A reassessment of TOPEX and Jason-1 altimetry based on revised reference frame and orbits. *Geophys. Res. Lett.*, 34, L14608, DOI:10.1029/2007GL030002.

Beckley, B.D., N.P. Zelensky, S.A. Holmes, F.G. Lemoine, R.D. Ray, G.T. Mitchum, S. Desai, S.T. Brown, Assessment of the Jason-2 Extension to the TOPEX/Poseidon, Jason-1 Sea-Surface Height Time Series for Global Mean Sea Level Monitoring, *Marine Geodesy*, 33(S1): 447-471, 2010, Supplemental Issue on OSTM/Jason-2 calibration/validation, Vol. 1, DOI: 10.1080/01490419.2010.491029.

Benada, J. R., 1997. "*PO.DAAC Merged GDR (TOPEX/POSEIDON) Generation B User's Handbook*", Version 2.0, JPL D-11007.

Bertiger W., Desai .S, Dorsey A., Haines B.J., Harvey N., Kuang D., Sibthorpe A., Weiss J.P. (2010) Sub-Centimeter Precision Orbit Determination with GPS for Ocean Altimetry, Marine Geodesy, Vol. 33, Iss. sup1, 2010

Bertiger W., Desai .S, Dorsey A., Haines B.J. et al., (2014), Time-Variable Gravity, Geocenter and Jason-2 Orbit Determination With GPS, OSTST POD oral presentation, Konstanz Germany, October 2014. http://www.aviso.altimetry.fr/en/user-corner/science-teams/ostst-swt-science-team.html

Brenner, A. C., C. J. Koblinsky, and B. D. Beckley. 1990. A Preliminary Estimate of Geoid-Induced Variations in Repeat Orbit Satellite Altimeter Observations. *J. Geophys. Res.,* 95(C3), 3033- 3040.

Brown, S., S. Desai, N. Lahaye, The End-of-Mission Climate Quality Calibration for the JMR, 2014 Ocean Surface Topography Science Team Meeting, Konstanz, Germany, http://meetings.aviso.altimetry.fr/fileadmin/user_upload/tx_ausyclsseminar/files/28Ball1400-3_OSTST_14_JMR_calibration_Brown.pdf

Carrère, L., and F. Lyard. 2003. Modelling the barotropic response of the global ocean to atmospheric wind and pressure forcing. *Geophys. Res. Lett.,* 30(6), art. 1275, DOI:10.1029/2002GL016473.

Cazenave, A., D.P. Chambers, P. Cipollini, L.L. Fu , et al., Sea Level Rise Regional And Global Trends, OCEANOBS2009- Plenary Paper (2009).

Cerri, L., F. Mercier, J.P. Berthias, J.C. Ries, F.G. Lemoine, N.P. Zelensky, et al., Precision orbit determination standards for the Jason series of altimeter missions. Part I, *Marine Geodesy* 33, 2010.

Collard F. and S. Labroue (2004), New Wind Speed Algorithm for Jason-1, Poster presented at the *OSTST Meeting*, November 2004, St Petersburg, Florida, USA.

Couhert, A., Cerri, L., Legais, J.F., et al. (2015), Towards the 1 mm/y stability of the radial orbit error at regional scales, Adv. Space Res., 55(1), 2-23, doi:10.1016/j.asr.2014.06.041

Chambers, D.P., S.A. Hayes, J.C. Ries, T.J. Urban. 2003. New TOPEX Sea State Bias Models and their Effect on Global Mean Sea Level. *J. Geophys Res*., 108, 3305.

Desai, S., J. Wahr, B. Beckley, Revisiting the pole tide for and from satellite altimetry, Journal of Geodesy, 89(8), 747-842, 2015. DOI 10.1007/s00190-015-0848-7

Gaspar, P., F. Ogor, P. Y. Le Traon, and O. Z. Zanife (1994), Estimating the sea state of the TOPEX and Poseidon altimeters from crossover differences, J. Geophys. Res., 99, 24,981 – 24,994.

Gaspar, P., and J.-P. Florens. 1998. Estimation of the sea state bias in radar altimeter measurements of sea level: Results from a new nonparametric method. *J. Geophys. Res.* 103:15803-15814.

Gaspar, P., S. Labroue, F. Ogor, G. Lafitte, L. Marchal, and M. Rafanel. 2002. Improving nonparametric estimates of the sea state bias in radar altimeter measurements of sea level. *J. Atmos. Oceanic Technol.* 19:1690-1707.

Goiginger, H., et al. (2011), The combined satellite-only global gravity field model GOCO02S, Geophysical Research Abstracts, 13, EGU2011–10,571.

Gourrion, J., D. Vandemark, S. Bailey, B. Chapron, G. P. Gommenginger, P. G. Challenor, and M. A. Srokosz (2002), A two-parameter wind speed algorithm for Ku-band altimeters, J. Atmos. Oceanic Technol., 19, 2030 – 2048.

King M.A. and C.S. Watson (2014), Geodetic vertical velocities affected by recent rapid changes in polar motion, Geophys. J. Int. (2014) 199, 1161–1165 doi: 10.1093/gji/ggu325

Kummerow, C. and W. Berg, A Fundamental Climate Data Record SSMI and SSMIS Science Data Stewardship, 2010 Workshop on Climate Data Records from Satellites, Silver Spring, MD, March 22-24, 2010. http://www.orbit.nesdis.noaa.gov/star/documents/meetings/CDR2010/talks/DayOne/Kummerow_C.pdf

Labroue, S., P. Gaspar, J. Dorandeu, O.Z. Zanife, F. Mertz, P. Vincent, and D. Choquet. 2004. Nonparametric estimates of the sea state bias for the Jason-1 radar altimeter. *Mar. Geod.* 27:453-481.

Lemoine, F.G., N.P. Zelensky, D.S. Chinn, D.E. Pavlis, D.D. Rowlands, B.D. Beckley**,** S.B. Luthcke, P. Willis, M. Ziebart, A. Sibthorpe, J. Boy, V. Luceri, Towards development of a consistent orbit series for TOPEX, Jason-1, and Jason-2, Adv. Space Research, 46 (2010) 1513-1540, doi: 10.1016/j.asr.2010.05.007

Lemoine, F.G., N. P. Zelensky, S. Melachroinos, D. S. Chinn, D. E. Pavlis, D.D. Rowlands, B.D. Beckley, R.D. Ray, S. B. Luthcke, Improved Orbit Standards for Altimeter Satellite POD at GSFC, POD Splinter oral presentation 2012 OSTST, Venice Italy.

Lemoine FG, Zelensky NP, Chinn DS, et al. (2014), New GSC POD Standards for TOPEX/Poseidon, Jason-1, Jason-2 (OSTM), OSTST POD oral presentation, Konstanz Germany, October 2014. http://www.aviso.altimetry.fr/en/user-corner/science-teams/ostst-swt-science-team.html

Lemoine, F.G., N.P. Zelensky, D.S. Chinn, B.D. Beckley, D.D. Rowlands, D.E. Pavlis (2015) A new time series of orbits (std1504) for TOPEX/Poseidon. Jason-1, and Jason-2 (OSTM), Ocean Surface Topography Science Team Meeting, Reston, VA. http://meetings.aviso.altimetry.fr/?id=95&nocache=1&tx_ausyclsseminar_pi2%5bobjAbstract%5d=1716&nocache=1&useCacheHash=1&cHash=1

Leuliette, E.W., and R. Scharroo, Integrating Jason-2 into a Multiple-Altimeter Climate Data Record, *Marine Geodesy*, 33(S1): 504-517, 2010, Supplemental Issue on OSTM/Jason-2 calibration/validation, Vol. 1, DOI: 10.1080/01490419.2010.487795.

Lyard, F., F. Lefevre, T. Letellier, and O. Francis, "Modeling the global ocean tides: Insights from FES2004", Ocean Dyn., 56, 394–415, 2006.

Marshall, J.A., Zelensky, N.P., Luthcke, S.B., Rachlin, K.E., Williamson R.G. (1995), The temporal and spatial characteristics of TOPEX/Poseidon radial orbit error*, J. Geophys Res*., *100(C12)*, pp. 25331-25352.

Melachroinos SA, Lemoine FG, Zelensky NP, Rowlands DD, Luthcke SB, Bordyugov O, The effect of geocenter motion on Jason-2 orbits and the mean sea level, Advances in Space Research, Volume 51, Issue 8, 15 April 2013, Pages 1323-1334, ISSN 0273-1177, http://dx.doi.org/10.1016/j.asr.2012.06.004.

Mitchum, G.T. 2000. An improved calibration of satellite altimetric heights using tide gauge sea levels with adjustment for land motion. *Marine Geodesy*, 23, 145-166.

Misra, S. and S. Brown, Application of a Mixed-Pixel Algorithm to TOPEX for Coastal Wet Tropospheric Delay Retrieval, 2011 Coastal Altimetry Workshop poster presentation.

Moreaux, G Willis P, Frank Lemoine F, Zelensky N, Couhert A, Hanane HAL, Ferrage P (2016), DPOD2014: a new DORIS extension of ITRF2014 for Precise Orbit Determination, 2016 AGU poster, http://ids-doris.org/documents/report/meetings/AGU2016_IDS_CC-DPOD2014-Moreaux.pdf

Nerem, R.S., D.P. Chambers, C. Choe, G.T. Mitchum, Estimating Mean Sea Level Change from the TOPEX and Jason Altimeter Missions, *Marine Geodesy*, 33(S1): 435-446, 2010, Supplemental Issue on OSTM/Jason-2 calibration/validation, Vol. 1, DOI: 10.1080/01490419.2010.491031.

OSTM/Jason-2 products handbook, Issue 1 rev 8, December 1, 2011. SALP-MU-M-OP-15815-CN(CNES), EUM/OPS-JAS/MAN/08/0041 (EUMETSAT), OSTM-29-1237 (JPL), Polar Series/OSTM J400 (NOAA/NESDIS).

Peltier, W. R., 2009. Closure of the budget of global sea level rise over the GRACE era: The importance and magnitude of the required corrections for global glacial isostatic adjustment, Quat. Sci. Rev. 17–18:1658–1674, doi:10.1016/j.quascirev.2009.04.004.

Picot, N., K. Case, S. Desai, and P. Vincent. 2008. *AVISO and PODAAC User Handbook. IGDR and GDR Jason Products, Edition 4.0*. SMM-MU-M5-OP-13184-CN (**AVISO**), JPL D-21352 (**PODAAC**).

Picot, N., et al., 2016, Jason-3 Products Handbook, Issue 1, revision 2, February 12, 2016, CNES : SALP-MU-M-OP-16118-CN

Ponte, R. M. and R. D. Ray, "Atmospheric pressure corrections in geodesy and oceanography: a strategy for handling air tides," Geophysical Research Letters, 29(24), 2153, 2002.

Ray, R. D. and D. E. Cartwright, "Satellite altimeter observations of the Mf and Mm ocean tides, with simultaneous orbit corrections," in Gravimetry and Space Techniques Applied to Geodynamics and Ocean Dynamics, pp. 69-78, American Geophysical

Union, Washington, 1994.Ray, R. D. and R. M. Ponte, "Barometric tides from ECMWF operational analyses," Annales Geophysicae, 21, 1897-1910, 2003.

Ray, R.D. 1999. A global ocean tide model from TOPEX/Poseidon altimetry: GOT99.2, NASA TM-1999-209478, NASA Goddard Space Flight Center, September 1999 (Update).

Ray, R.D., B.D. Beckley, F.G. Lemoine. Vertical crustal motion derived from satellite altimetry and tide gauges, and comparisons with DORIS measurements. Adv. Space Research, 45 (2010) 1510-1522, doi: 10.1016/j.asr.2010.02.020

Ries JC (2013), Annual Geocenter Motion from Space Geodesy and Models, G12A-08, presented at 2013 Fall AGU Meeting, San Francisco, CA, 9-13 December 2013. http://ids-doris.org/report/publications/on-line-publications.html#geodesy

Rudenko S, Dettmering D, Esselborn S, Schoene T, Foerste C, Lemoine J-M, Ablain M, Alexandre D, Neumayer K-H (2014) Influence of time variable geopotential models on precise orbits of altimetry satellites, global and regional mean sea level trends. Advances in Space Research, doi: 10.1016/j.asr.2014.03.010

Santamaría-Gómez, A., M. Gravelle, X. Collilieux, M. Guichard, B. Martín Míguez, P. Tiphaneau, and G. Wöppelmann (2012), Mitigating the effects of vertical land motion in tide gauge records using state-of-the-art GPS velocity field, Global Planet. Change, 98-99, 6–17.

Schrama, E. J. O. and R. D. Ray, "A preliminary tidal analysis of TOPEX/Poseidon altimetry," Journal of Geophysical Research, 99, 24799-24808, 1994.

Stammer, D., R.D. Ray, O.B. Andersen, et al., Accuracy assessment of global barotropic ocean tide models, Reviews of Geophysics, 2014.

TOPEX Ground System Science Algorithm Specification, JPL D-7075, Rev. A, Change 1; April 25, 1991.

Tran, N., Phillips, E. Bronner, and N. Picot, Impact of GDR_D standards on SSB corrections, Ocean Surface Topography Science Working Team Meeting, Venice, Italy, 2012. http://www.aviso.oceanobs.com/fileadmin/documents/OSTST/2012/oral/02_friday_28/01_instr_processing_I/01_IP1_Tran.pdf

Tran, N., S. Labroue, S. Phillips, E. Bronner, and N. Picot, Overview and Update of the Sea State Bias Corrections for the Jason-2, Jason-1, and TOPEX Missions. *Mar. Geod.* 33(S1): 348-362, 2010. DOI: 10.1080/01490419.2010.487788

Wöppelmann, G., C. Letetrel, A. Santamaria, M.-N. Bouin, X. Collilieux, Z. Altamimi, S.D.P. Williams, B. Martin Miguez, 2009. Rates of sea-level change over the past century in a geocentric reference frame. Geophys. Res. Lett. 36, L12607, 2009.

Zelensky, N.P., F.G. Lemoine, M. Ziebart, A. Sibthorpe, P. Willis, B.D. Beckley, S.M. Klosko, D.S. Chinn, D.D. Rowlands, S.B. Luthcke, D.E. Pavlis, V. Luceri (2010), DORIS/SLR

POD modeling improvements for Jason-1 and Jason-2, Adv. Space Research, 46(12), 1541-1558, 2010. doi: 10.1016/j.asr.2010.05.008

Zelensky, N.P., F. G. Lemoine, B. Beckley, D. S. Chinn, S. Melachroinos, S. B. Luthcke G. Mitchum, O. Bordyugov, Improved Modelling of Time-Variable Gravity for Altimeter Satellite POD (2012), POD Splinter poster 2012 OSTST, Venice Italy.

Zelensky, N.P., F. G. Lemoine, S. Melachroinos, D. S. Chinn, B. Beckley, D.E. Pavlis, J. Wimert (2014), Impact of atmosphere loading and geocenter motion station corrections on the Jason-2 and Envisat SLR+DORIS orbits , POD Splinter, 2014 OSTST, Konstanz Germany.

Zelensky, N.P., F. G. Lemoine, D. S. Chinn, B. Beckley, D.E. Pavlis (2016), New SLR-based geocenter estimates for orbit centering and impact on altimeter sea surface analysis, POD Splinter 2016 OSTST, La Rochelle France.

# Appendix I: Quality Flag Bit Distributions

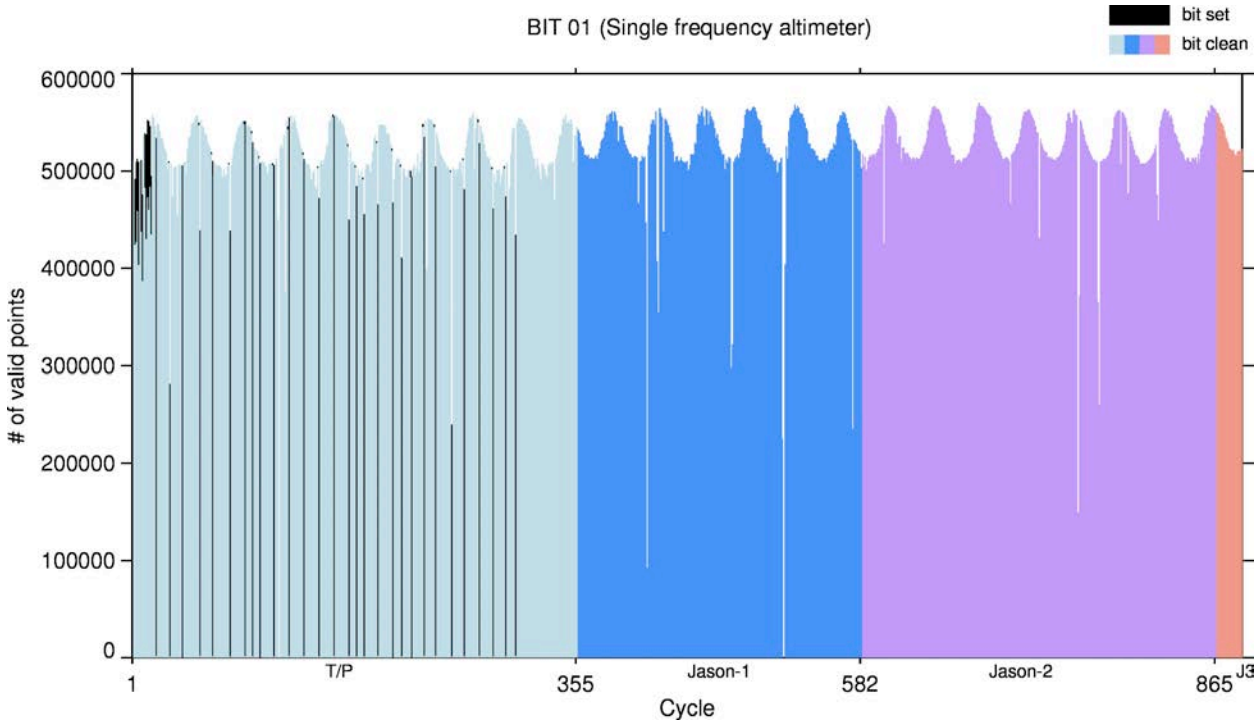


**Figure A-1: Quality flag word Bit #1 when set to 1 indicates Poseidon-1 (single frequency) altimeter observations.**

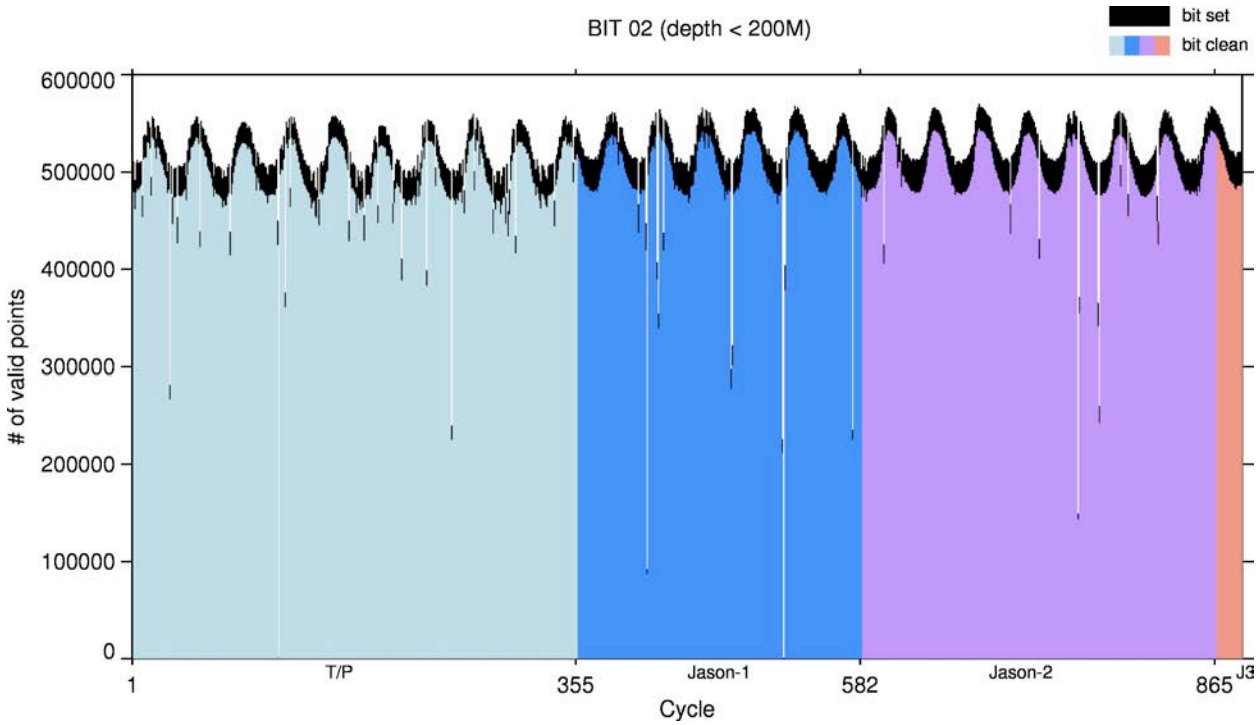


**Figure A-2: Quality flag word Bit #2 when set to 1 indicates locations where ocean depth < 200 m.**

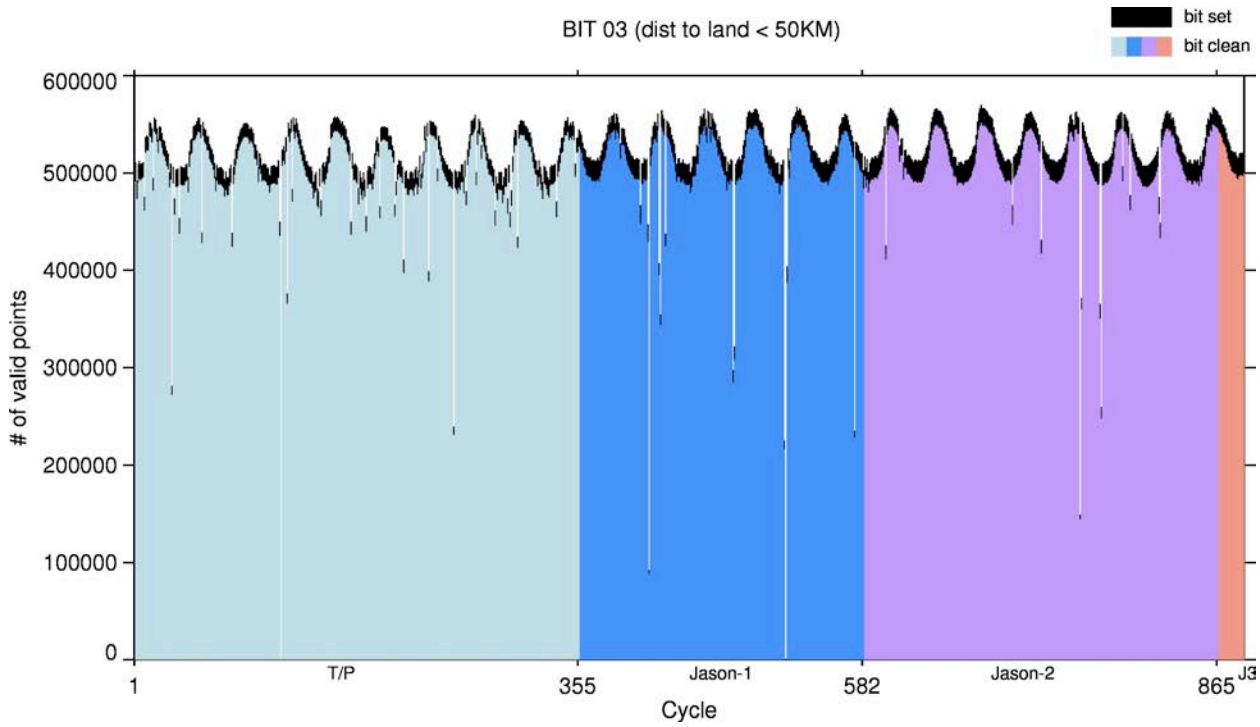


**Figure A-3: Quality flag word bit #3 when set to 1 indicates locations within 50 km to coastline.**

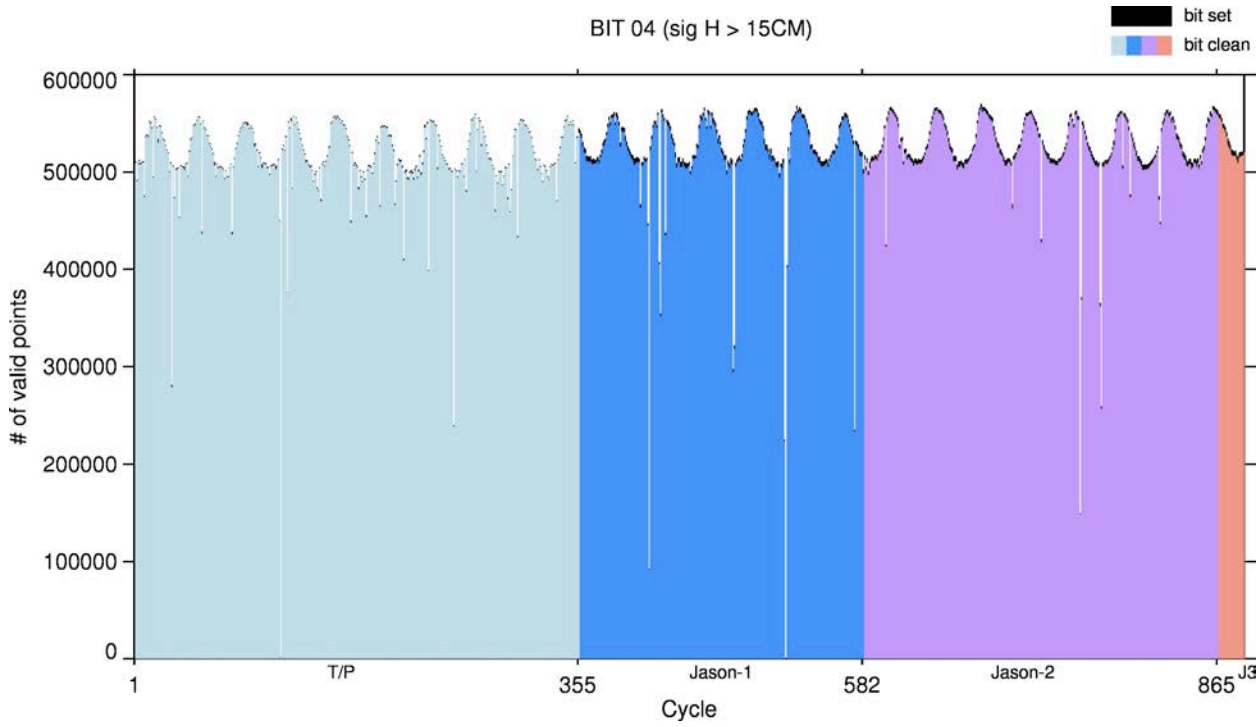


**Figure A-4: Quality flag word bit #4 when set to 1 identifies 1Hz SSH measurements with standard deviation of high rate SSH residuals with respect to 1Hz "average" is grater than 15 cm (20 cm for Poseidon-1).**

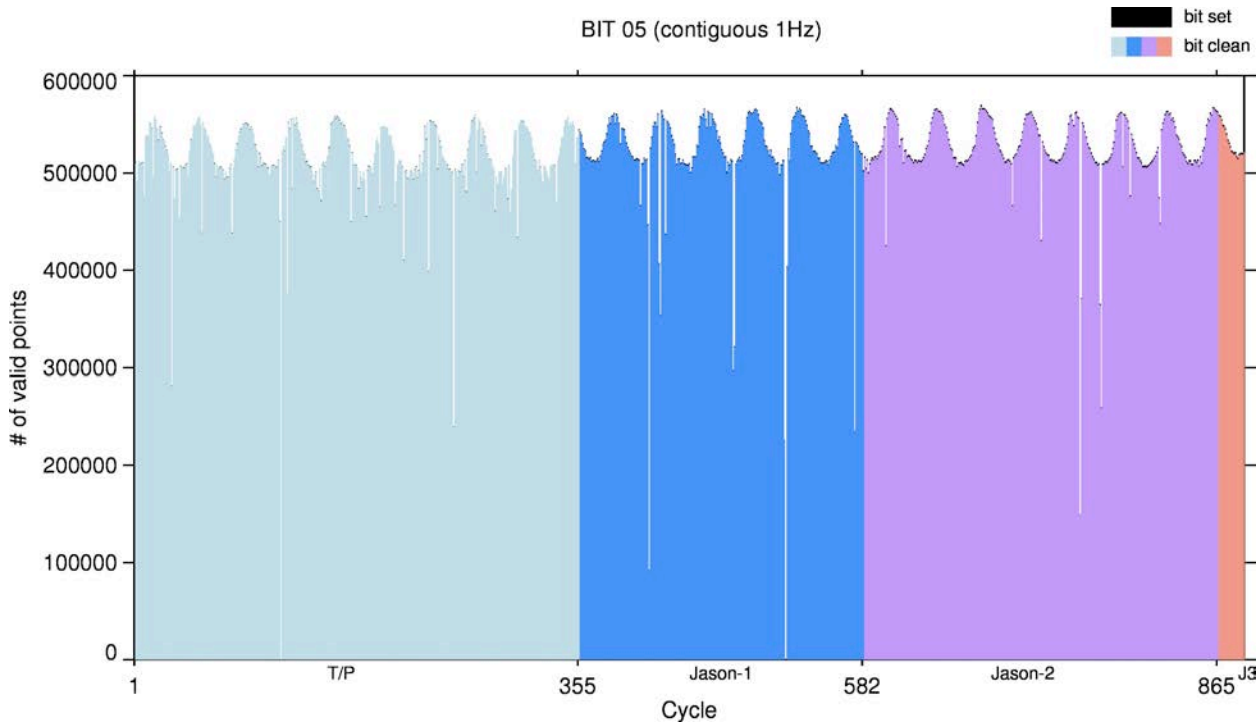


**Figure A-5: Quality flag word bit #5 when set to 1 identifies 1Hz geo-referenced SSH values not derived from a nominal contiguous pair of high rate SSH measurements.**

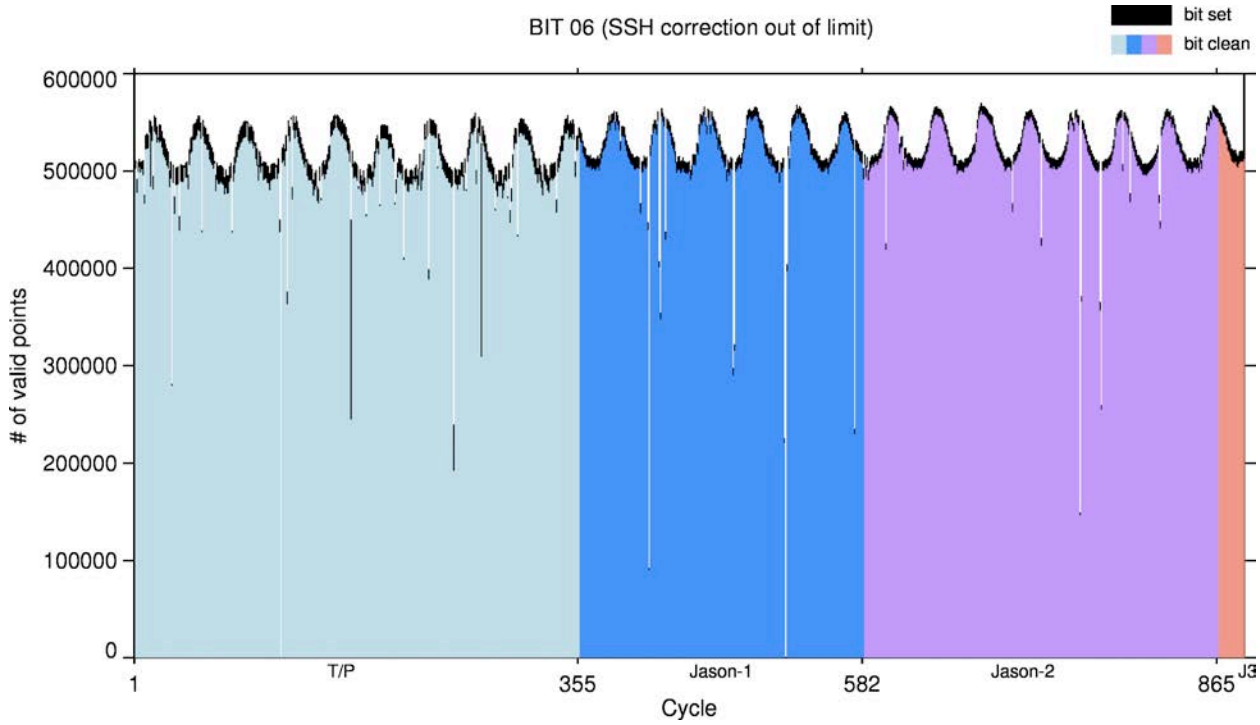


**Figure A-6: Quality flag word bit #6 when set to 1 identifies valid (not equal to 32767) 1Hz geo-referenced SSH with one or more range or geophysical corrections outside nominal limits (see table 2).**

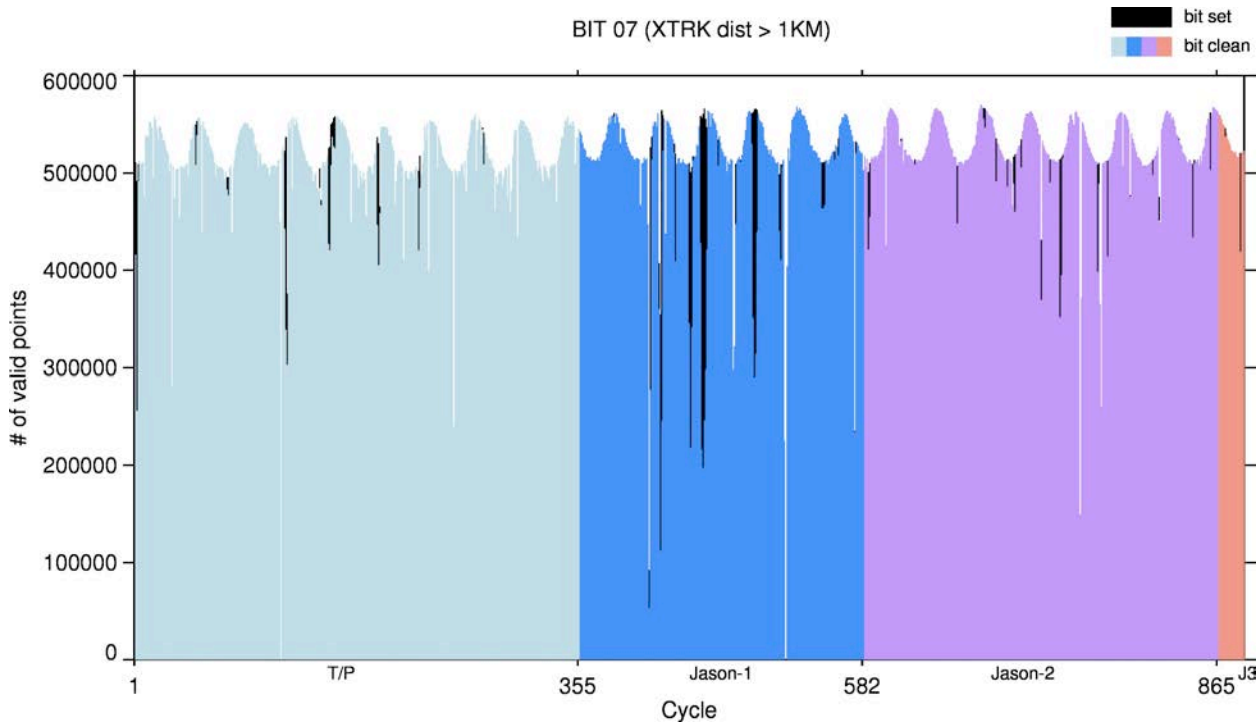


**Figure A-7: Quality flag word bit #7 when set to 1 identifies locations with a cross-track distance > 1 km with respect to reference orbit.**

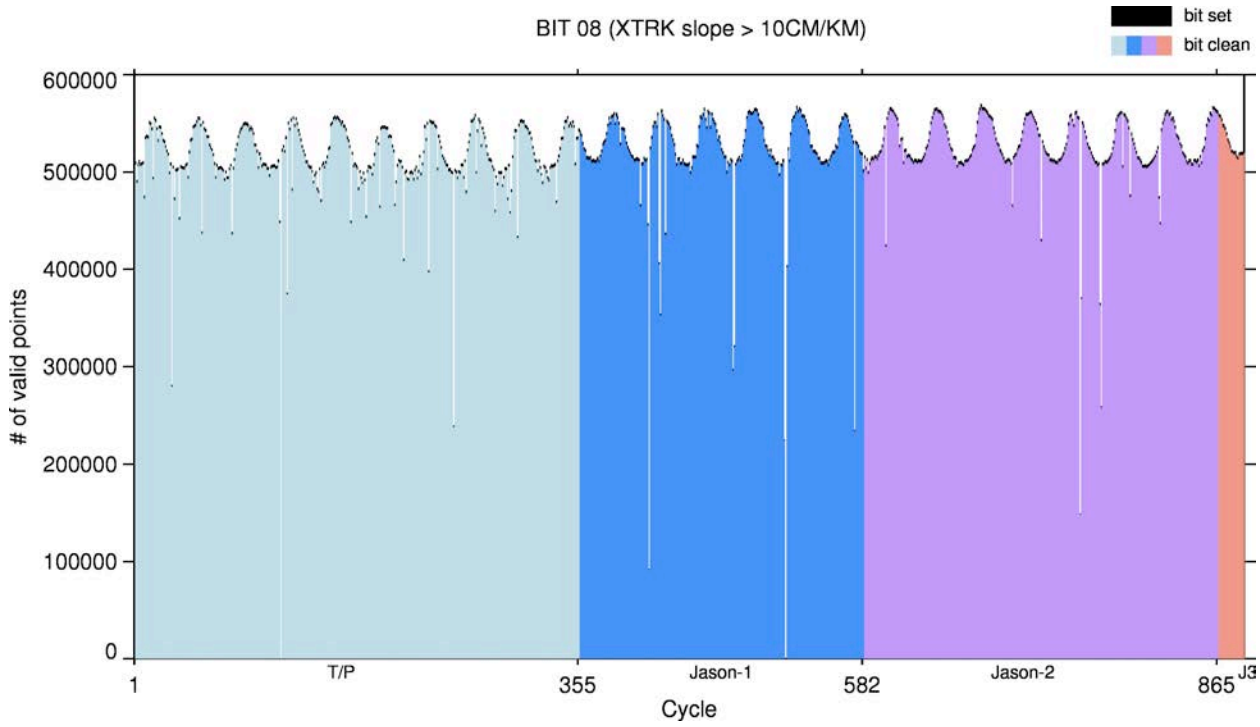


**Figure A-8: Quality flag word bit #8 when set to 1 identifies locations with cross track geoid gradients exceeding 10 cm/km.**

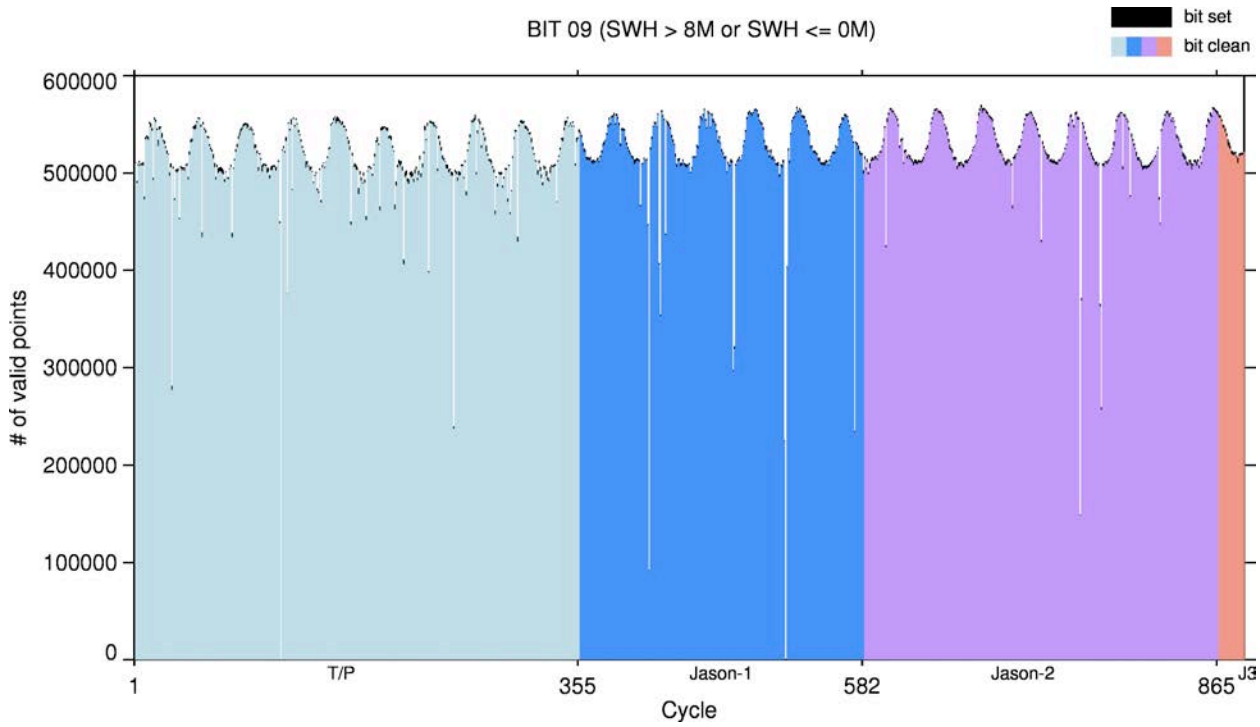


**Figure A-9: Quality flag word bit #9 when set to 1 indicates SSH measurements at high sea states with SWH_Ku greater than 8.0 m, less than or equal to 0m.**

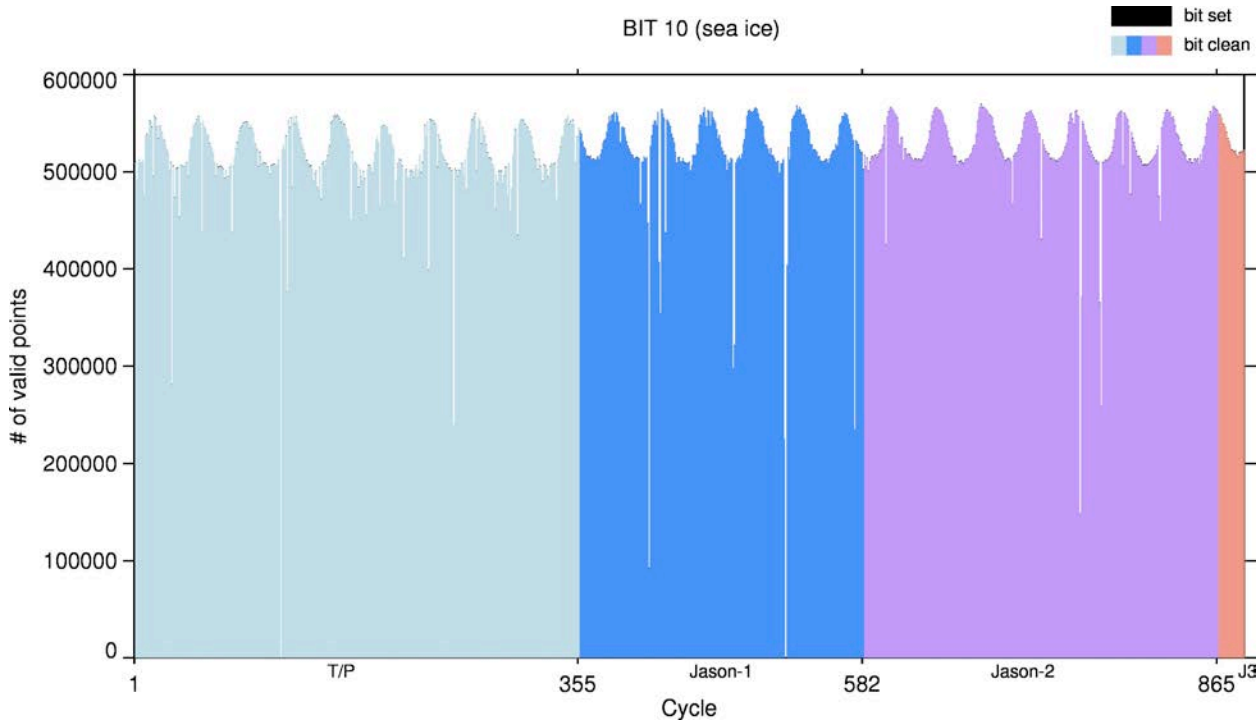


**Figure A-10: Quality flag word bit #10 when set to 1 indicates observations with possible contamination of SSH estimate from presence of sea ice.**

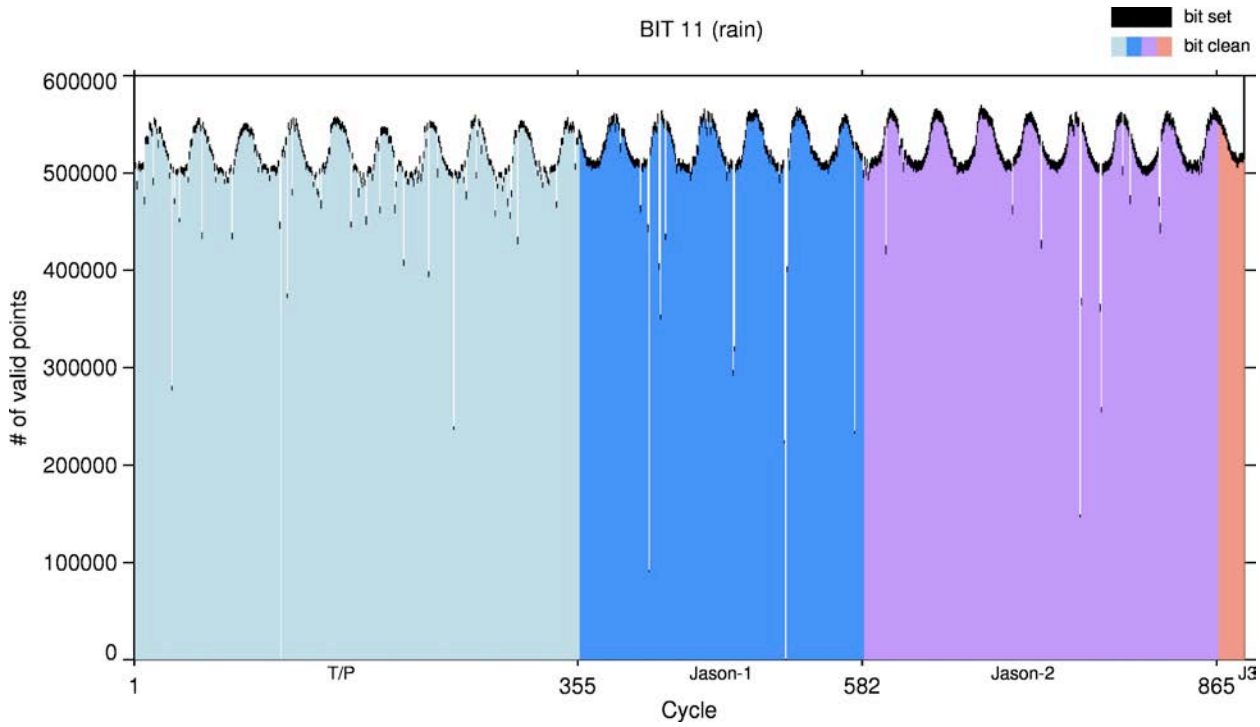


**Figure A-11: Quality flag word bit 11 when set to 1 indicates observations with possible contamination of SSH estimate due to presence of rain. Current algorithm specifications for rain/sea ice detection are in Appendix II below.**

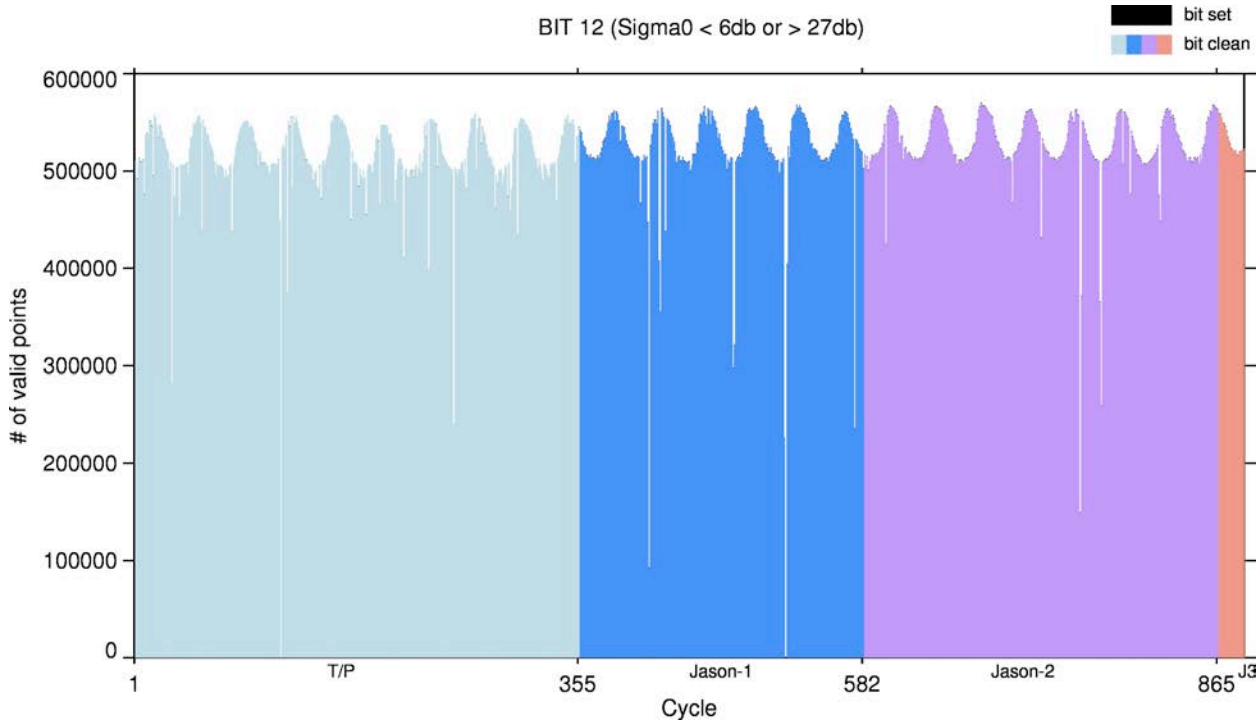


**Figure A-12: Quality flag word bit #12 when set to 1 identifies observations with backscatter coefficients outside nominal range indicating high wind conditions or possible land/ice contamination.**

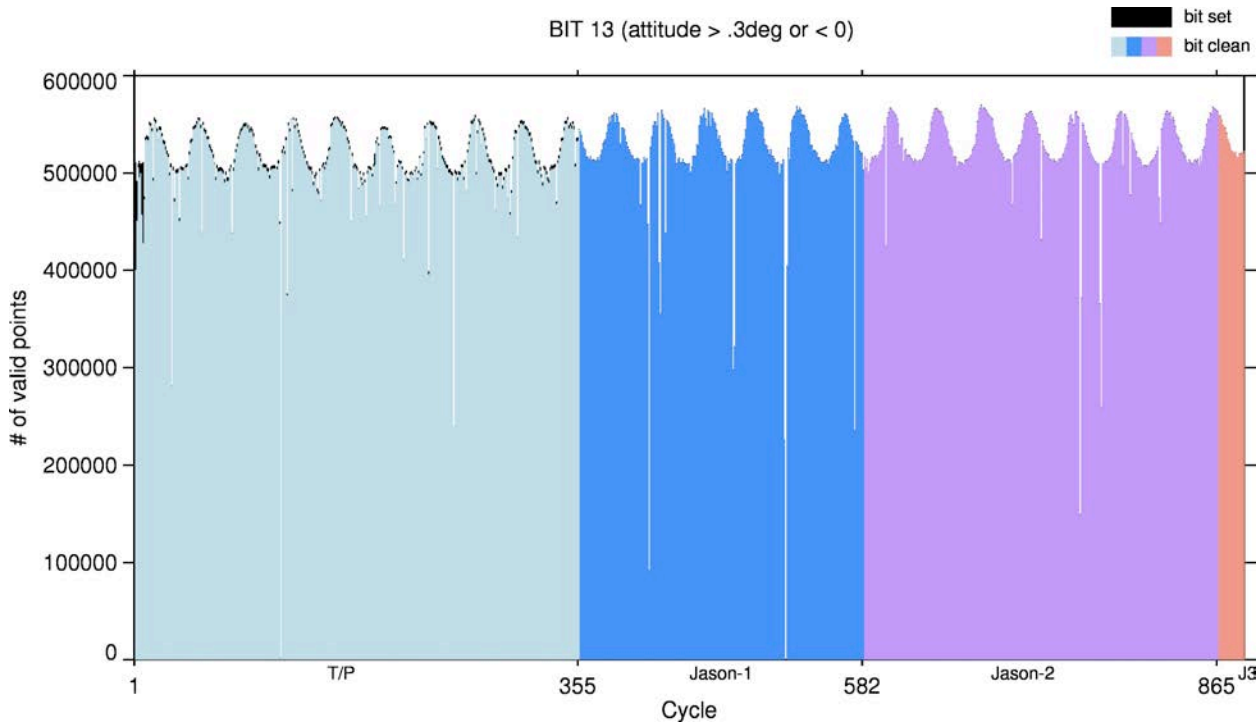


**Figure A-13: Quality flag word bit #13 when set to 1 identifies observations when the attitude_waveform is outside nominal range limits.**

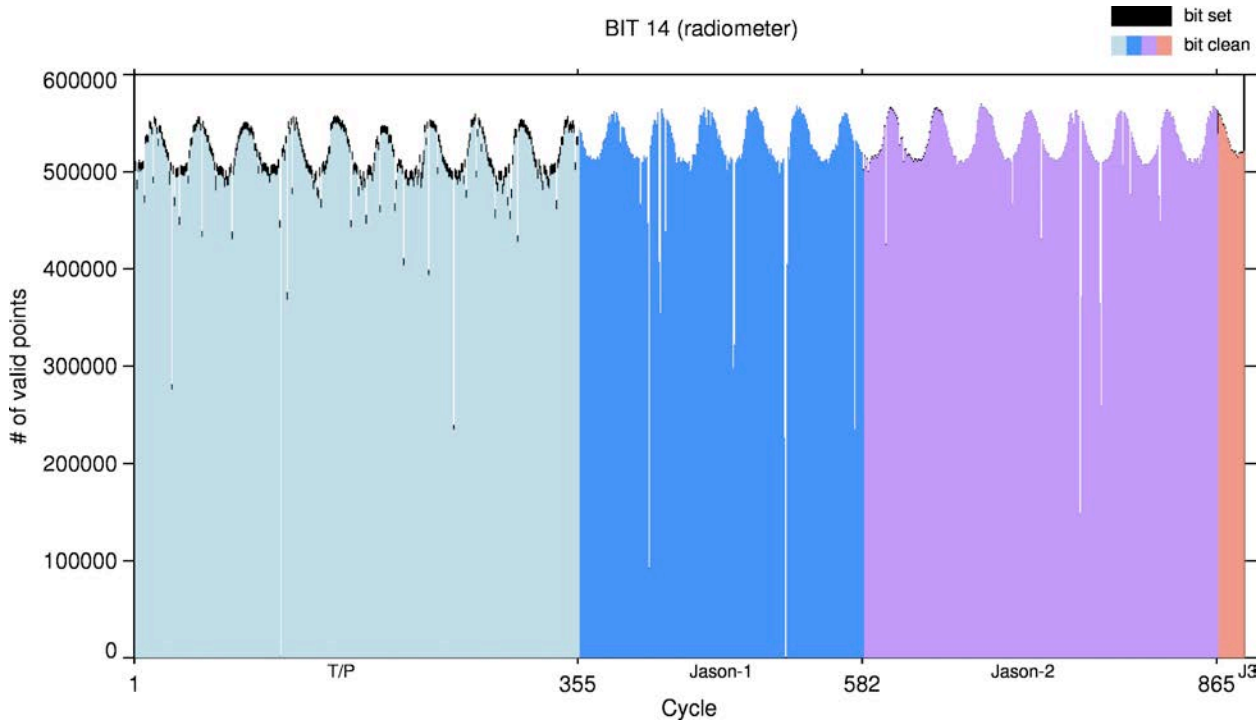


**Figure A-14: Quality flag word bit #14 when set to 1 indentifies observations where the radiometer measurement is believed to be suspect.**

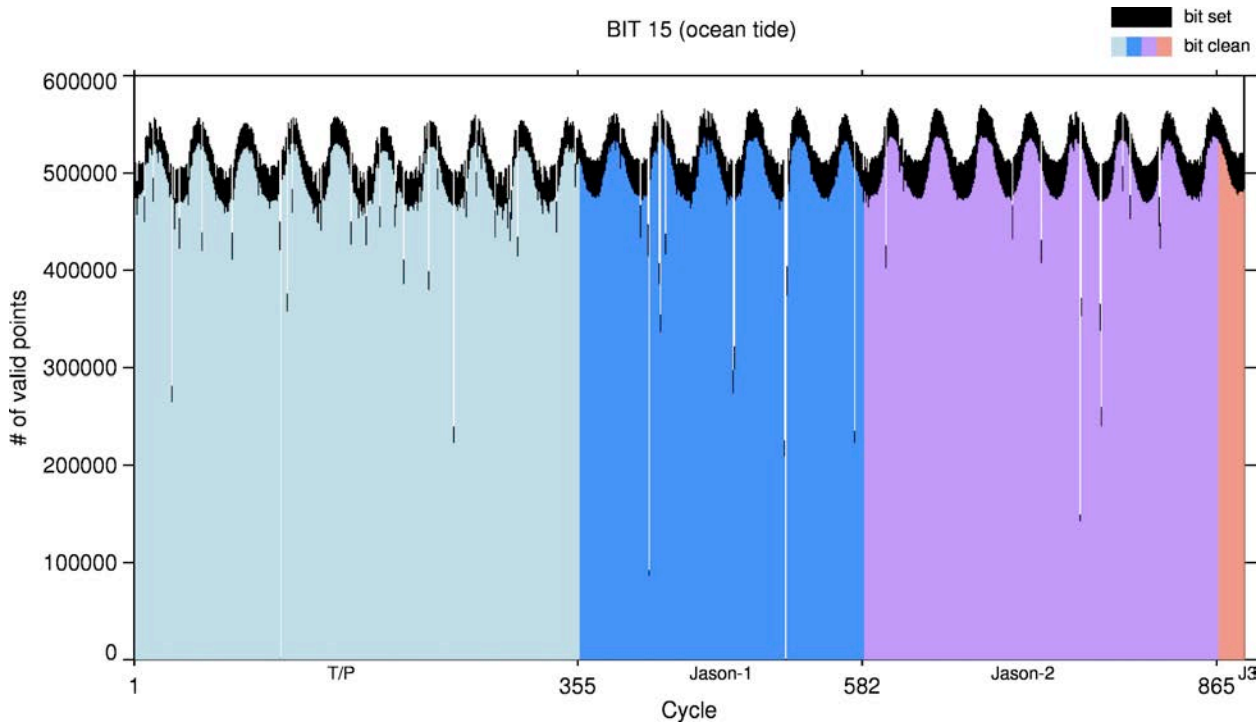


**Figure A-15: Quality flag word bit #15 when set to 1 identifies coastal locations where the mean GOT4.8/FES04 ocean tide correction differs by more than 2.0 cm (see figure 20).**

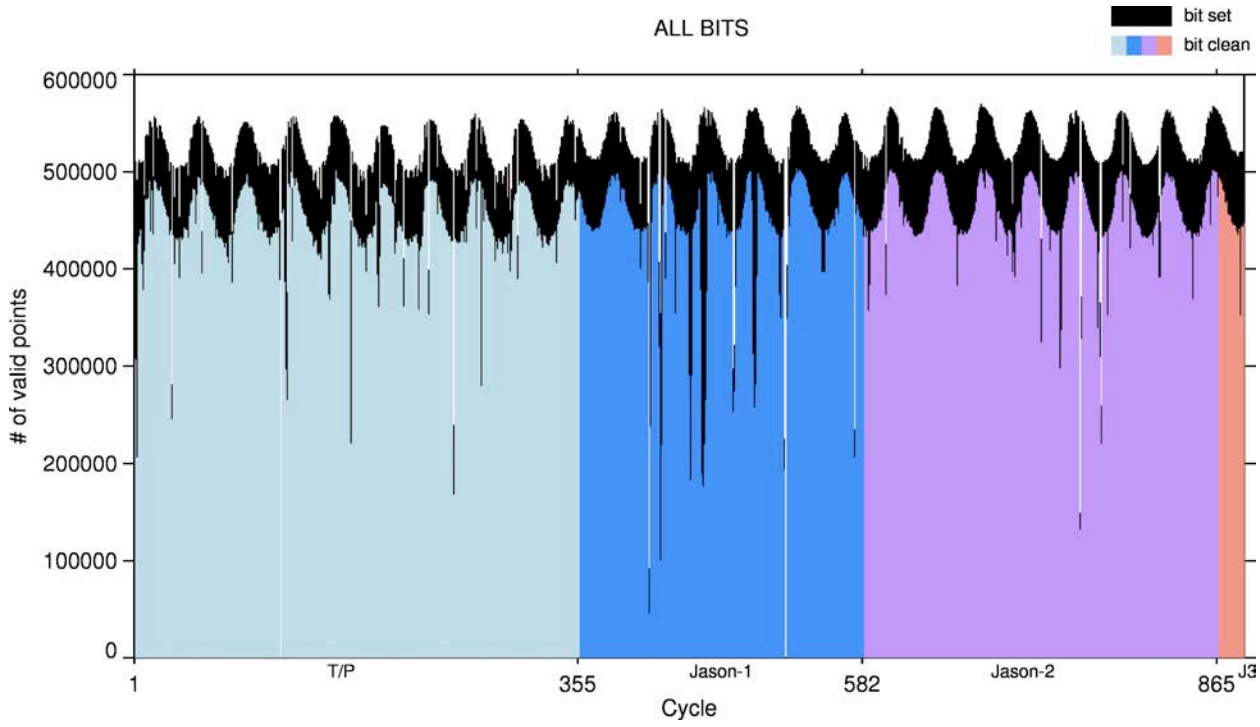


**Figure A-16: An edit strategy that requires all bits set to 0 (except bit #1 to retain Poseidon-1 data) will result in ~ 10 % data loss.**

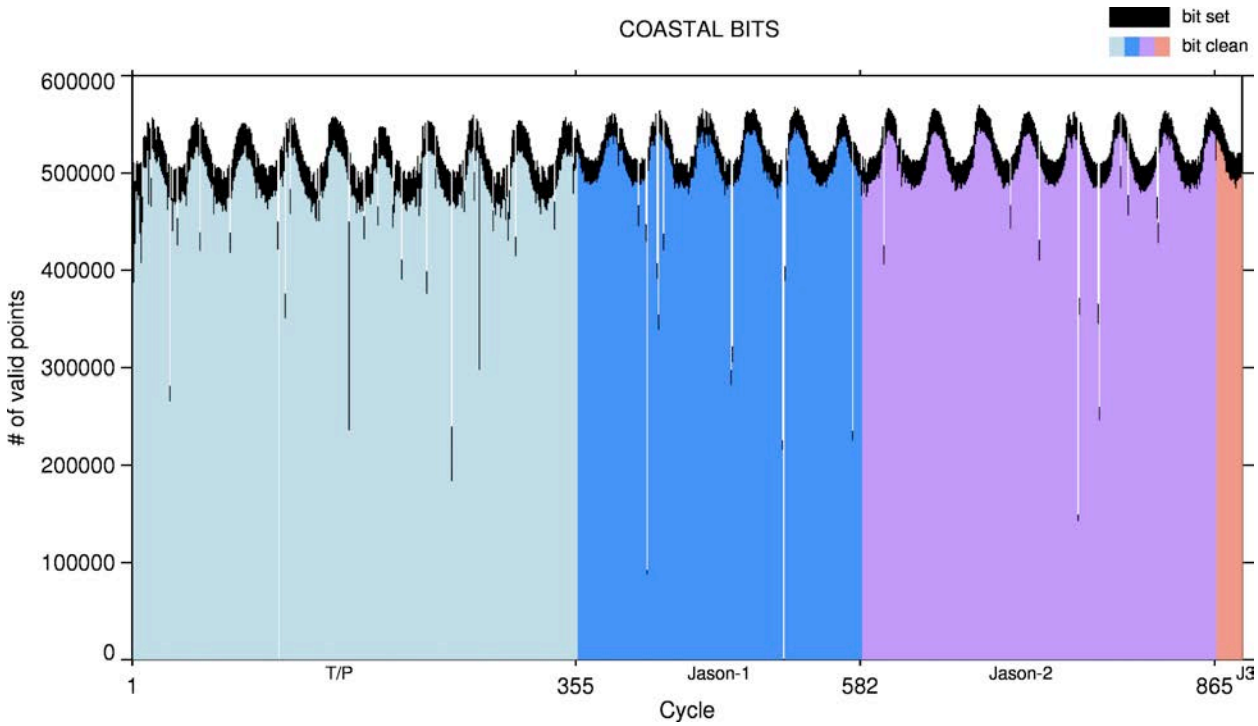


**Figure A-17: Edit strategy as above except coastal observations are retained (bits 2,3, and 15) and both bits 7&8 in combination must be set, resulting in ~ 5 % data loss.**

# Appendix II: Sea State Bias Specifications

Jason-2&3: ssb_col_J2_Ku_mle4_1_36_v2012ostst.rs (Tran et al., 2012.)

Jason-1: ssb_col_J1_1_111_v2012ostst.rs (Tran et al., 2010)

TOPEX Side A: ssb_col_TPmgdr_021_131_v2009.rs (Tran et al., 2010)

TOPEX Side B: ssb_col_TPmgdr_240_350_v2009.rs (Tran et al., 2010)